Euro. Jnl of Applied Mathematics (2021), *vol.* 32, *pp.* 242–279
doi:10.1017/S095679252000011X

Extended Stefan problem for the solidification of binary alloys in a sphere

FERRAN BROSA PLANELLA[1], COLIN P. PLEASE[2] and ROBERT A. VAN GORDER[3]

[1]*WMG, University of Warwick, Gibbet Hill Road, Coventry CV4 7AL, UK*
[2]*Mathematical Institute, University of Oxford, Andrew Wiles Building, Radcliffe Observatory Quarter, Woodstock Road, Oxford OX2 6GG, UK*
[3]*Department of Mathematics and Statistics, University of Otago, P.O. Box 56, Dunedin 9054, New Zealand*
email: rvangorder@maths.otago.ac.nz

(*Received 13 October 2019*; *revised 12 March 2020*; *accepted 30 March 2020*; *first published online 4 May 2020*)

We study the extended Stefan problem which includes constitutional supercooling for the solidification of a binary alloy in a finite spherical domain. We perform an asymptotic analysis in the limits of large Lewis number and small Stefan number which allows us to identify a number of spatio-temporal regimes signifying distinct behaviours in the solidification process, resulting in an intricate boundary layer structure. Our results generalise those present in the literature by considering all time regimes for the Stefan problem while also accounting for impurities and constitutional supercooling. These results also generalise recent work on the extended Stefan problem for finite planar domains to spherical domains, and we shall highlight key differences in the asymptotic solutions and the underlying boundary layer structure which result from this change in geometry. We compare our asymptotic solutions with both numerical simulations and real experimental data arising from the casting of molten metallurgical grade silicon through the water granulation process, with our analysis highlighting the role played by supercooling in the solidification of binary alloys appearing in such applications.

Key words: Two-phase Stefan problem, solidification of binary alloys, matched asymptotic analysis

2020 Mathematics Subject Classification: Primary: 80A22; 35R37. Secondary: 34E10; 80A20

1 Introduction

The process of solidification arises in a variety of applications, both in the natural sciences and in industry. Many solidification processes can be modelled using Stefan problems [25, 35, 38] which, except in very particular cases, do not admit closed-form analytical solutions, motivating a variety of analytical and numerical approaches. We can distinguish between one-phase and two-phase Stefan problems, and in the literature, the former has received a lot of attention. One of the usual analytical approaches is to use asymptotic techniques to determine approximate solutions to it. A common asymptotic limit to consider is where the Stefan number is large, corresponding to the situation where latent heat dominates, with a variety of geometries being studied [23, 28, 29, 34, 37, 39, 44]. Asymptotics for the small-time behaviour [5, 9, 18, 19] and end-time behaviour [28, 29, 34, 37, 39] are well studied for the one-phase problem. In addition to

asymptotic analysis, various numerical approaches for solving one-phase Stefan problems have been considered [1, 7, 8, 26, 27, 36, 40]. The asymptotic analysis of the solidification of spheres was first considered by Pedroso and Domoto [33], with asymptotic solutions of the one-phase Stefan problem in a sphere obtained in the small Stefan number limit (latent heat dominated). This analysis was subsequently extended and refined [34, 39, 37], requiring the consideration of several layers in the problem. A more general asymptotic analysis for the one-phase Stefan problem in an arbitrary three-dimensional geometry near the end of the solidification process was later considered [29].

Despite many applications, analysis of the corresponding two-phase Stefan problem is more mathematically involved and as a result has received less attention. There are some results for the two-phase Stefan problem in cylindrical or spherical domains [22, 24, 20]. A comprehensive analysis of the two-phase Stefan problem for a sphere was given by McCue et al. [30], which gave an exponentially small correction in the small timescale. The inward solidification of a binary alloy in a sphere was considered by Yang et al. [48], and however, only the well-mixed limit was considered, valid for when concentration and temperature profiles are spatially uniform. As such, their model is equivalent to a one-phase Stefan problem with a supercooling condition that depends on the position of the interface. The two-phase Stefan problem with constitutional supercooling in a sphere was studied in [15], which includes an asymptotic analysis of the small-time regime, yet the late-time dynamics were only discussed qualitatively with no formal analysis was provided. Such results, while qualitatively useful in some regimes, neglect the full boundary layer structure which naturally emerges from this problem. On the numerical side, these problems have been addressed using many different techniques, such as the enthalpy method [8, 43], interface-tracking methods [16, 45], phase-field methods [46, 47] and level-set methods [6, 41]. A detailed review of these techniques can be found in [21].

In the present paper, we perform an asymptotic analysis in order to study the extended Stefan problem for a binary alloy with constitutional supercooling in a spherical domain, in the limits of large Lewis number and small Stefan number. We assume that the diffusivity of impurities in the solid, segregation coefficient and initial concentration and temperature are small while the supercooling coefficient is large, meaning that a large concentration of impurities is required to cause a significant change in the solidification temperature. Such assumptions are relevant to real-world applications, such as the solidification of metallurgical grade silicon. Analysis of this problem shows the existence of a complicated boundary layer structure, which we exploit for our asymptotic analysis. Our results generalise various results in the literature [15, 30, 37] by considering all time regimes in the Stefan problem with impurities and constitutional supercooling. Due to their definition of the Stefan number, the analysis in those papers corresponds to the large Stefan number limit (i.e. the case when the problem is dominated by latent heat). A similar physical problem was recently studied in planar domains in which the solidification fronts remain flat [4]. However, many real-world solidification problems take place in domain geometries which involve curvature, and the present paper constitutes an extension of the results of Brosa Planella et al. [4] to curved domains. In particular, the choice of a spherical domain corresponds well to the solidification of droplets under the water granulation process. While the early-time dynamics are similar between the flat and curved domains, we find that there are fundamental differences between the late-time dynamics leading to extinction, and hence the related boundary layer structure when curvature is involved, necessitating a separate and more nuanced analysis from that of the planar geometry [4].

https://doi.org/10.1017/S095679252000011X Published online by Cambridge University Press

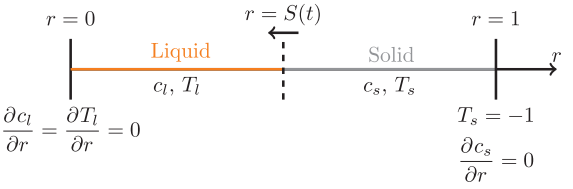

FIGURE 1. Sketch of the sphere solidification problem. As the problem is symmetric, we can just consider a one-dimensional problem with a symmetry condition at $r = 0$.

The remainder of this paper is organised as follows. In Section 2, we present the model for the solidification of a sphere. Our asymptotic analysis in the large Lewis number limit reveals eight different layers which are studied in Sections 3–6 and then matched together through the method of matched asymptotic expansions. All of these asymptotic results are summarised and discussed in Section 7, where we also compare the asymptotic solutions to direct numerical simulations of the full problem and also to experimental data from the solidification of silicon under the water granulation process. We conclude with a discussion of the results in Section 8.

2 Model for the solidification of a sphere

We study the solidification of a binary alloy in a three-dimensional spherically symmetric geometry. Recall that, as we have assumed spherical symmetry, the problem can be reduced to a one-dimensional model in the radial coordinate with the geometry shown in Figure 1. Our application of interest is metallurgical grade silicon, which is composed of over 99% silicon with the remaining being different types of impurities. In our model, we consider all impurities together as a single phase, and we use a binary alloy model to describe the system. In keeping with our application of interest, for the rest of the paper, we refer to the base of the alloy as silicon and we refer to the solutes as impurities.

We take the general model for the solidification of a binary alloy in an arbitrary domain presented in [4] and derive from it the model for a solidification of a spherically symmetric problem. This model is composed of four diffusion equations (for heat and impurities in both the solid and liquid phases) and five boundary conditions in the moving boundary which impose continuity of temperature, thermodynamic equilibrium using a linear phase diagram, conservation of heat and conservation of mass through the boundary. We take the independent variables r for the radial coordinate and t for time. Then, we define the following unknowns which depend on r and t: concentrations of impurities c_s and c_l and the temperatures T_s and T_l, where the subscripts s and l denote the solid and liquid phases, respectively. We also define the position of the interface $S(t)$, so we define $f_i = r - S(t)$ in the model in [4]. Finally, we take the differential operator ∇ to be for a spherically symmetric geometry.

Then, the general model in [4] reduces to the following. For the solid phase, which is given by $S(t) < r < 1$, the dimensionless model reads

$$\frac{\partial c_s}{\partial t} = \frac{D}{\mathrm{Le}} \frac{1}{r^2} \frac{\partial}{\partial r} \left(r^2 \frac{\partial c_s}{\partial r} \right), \quad \frac{\partial T_s}{\partial t} = \kappa \frac{1}{r^2} \frac{\partial}{\partial r} \left(r^2 \frac{\partial T_s}{\partial r} \right). \tag{2.1a}$$

https://doi.org/10.1017/S095679252000011X Published online by Cambridge University Press

The liquid phase is given by $0 < r < S(t)$, and the equations in this region of the domain are

$$\frac{\partial c_l}{\partial t} = \frac{1}{\mathrm{Le}}\frac{1}{r^2}\frac{\partial}{\partial r}\left(r^2\frac{\partial c_l}{\partial r}\right), \quad \frac{\partial T_l}{\partial t} = \frac{1}{r^2}\frac{\partial}{\partial r}\left(r^2\frac{\partial T_l}{\partial r}\right). \tag{2.1b}$$

The interface is given by $r = S(t)$, and the interface conditions reduce to

$$T_s = T_l, \quad c_s = \alpha c_l, \quad c_l = -m_l T_l, \quad \frac{\rho}{\mathrm{St}}\frac{\mathrm{d}S}{\mathrm{d}t} = k\frac{\partial T_s}{\partial r} - \frac{\partial T_l}{\partial r},$$
$$\text{and} \quad (1-\alpha)c_l\frac{\mathrm{d}S}{\mathrm{d}t} = \frac{D}{\mathrm{Le}}\frac{\partial c_s}{\partial r} - \frac{1}{\mathrm{Le}}\frac{\partial c_l}{\partial r}. \tag{2.1c}$$

The boundary and initial conditions are given by

$$\frac{\partial T_l}{\partial r} = 0 \quad \text{and} \quad \frac{\partial c_l}{\partial r} = 0, \ \text{at } r = 0, \qquad T_s = -1 \quad \text{and} \quad \frac{\partial c_s}{\partial r} = 0, \ \text{at } r = 1, \tag{2.1d}$$

$$S = 1, \quad T_l = T_0, \quad \text{and} \quad c_l = c_0, \ \text{at } t = 0. \tag{2.1e}$$

The dimensionless parameters are as defined in [4], where St is the Stefan number and Le is the Lewis number. The following dimensional values are defined as the ratio between the value of the parameter in the solid phase over the value in the liquid phase: D is the diffusivity of impurities, κ is the thermal diffusivity, ρ is the density and k is the thermal conductivity. Finally, m_l is the dimensionless supercooling coefficient and α is the segregation coefficient, and both come from the dimensionless phase diagram. As discussed in the derivation of the model in [4], we consider different values of densities in each phase for their contribution to the heat diffusivity but assume that both the solid and liquid phases are stationary. Therefore, we do not consider the advection introduced to the system by this variation in density and note that by neglecting this we are effectively working in the regime $\rho \approx 1$. We later fix $\rho = 1$ when plotting our asymptotic solutions and performing numerical simulations.

Similarly to Brosa Planella et al. [4], we are interested in the limit of very large Lewis number. However, as could be expected from the results in the literature [30, 37, 39], in order to find analytical solutions, we need to take the limit of small Stefan number as well. In our analysis, we first take the large Lewis number limit. For convenience, as we did in the planar geometry case, we write $\epsilon = \mathrm{Le}^{-1}$ and consider the limit $\epsilon \to 0$. We then take the limit $\mathrm{St} \to 0$. We will show later that this procedure is valid provided $\epsilon^{\frac{2}{3}} \ll \mathrm{St}$, which is true in our problem. The validity of this distinguished limit between the two small parameters is discussed in Section 4. The rest of the parameters are scaled as $D = \epsilon\hat{D}$, $m_l = \frac{\hat{m}_l}{\epsilon}$, $\alpha = \epsilon\hat{\alpha}$, $c_0 = \epsilon\hat{c}_0$, $T_0 = \epsilon\hat{T}_0$, where $\hat{D}$, $\hat{m}_l$, $\hat{\alpha}$, $\hat{c}_0$, and $\hat{T}_0$ are all order one. By setting these scalings, we are not implying that all the parameters above are related physically to Le. Rather, we are using ϵ as an order parameter and choosing the scaling with ϵ based on order-of-magnitude requirements for each parameter. The order one hat-parameters then hold information on the specific reference value of that parameter. In this way, we reduce the number of independent small or large parameters in the system, making the problem amenable to analysis. These hat-parameter scalings are chosen from the typical parameter values for the cast of metallurgical grade silicon, which can be found in [3].

We can write the rescaled dimensionless model as

$$\frac{\partial c_s}{\partial t} = \epsilon^2\hat{D}\left(\frac{\partial^2 c_s}{\partial r^2} + \frac{2}{r}\frac{\partial c_s}{\partial r}\right), \quad \frac{\partial T_s}{\partial t} = \kappa\left(\frac{\partial^2 T_s}{\partial r^2} + \frac{2}{r}\frac{\partial T_s}{\partial r}\right), \quad \text{for } S(t) < r < 1, \tag{2.2a}$$

https://doi.org/10.1017/S095679252000011X Published online by Cambridge University Press

$$\frac{\partial c_l}{\partial t} = \epsilon \left(\frac{\partial^2 c_l}{\partial r^2} + \frac{2}{r} \frac{\partial c_l}{\partial r} \right), \quad \frac{\partial T_l}{\partial t} = \frac{\partial^2 T_l}{\partial r^2} + \frac{2}{r} \frac{\partial T_l}{\partial r}, \quad \text{for } 0 < r < S(t), \tag{2.2b}$$

$$T_s = T_l, \quad c_s = \epsilon \hat{\alpha} c_l, \quad \epsilon c_l = -\hat{m}_l T_l, \quad \frac{\rho}{\mathrm{St}} \frac{\mathrm{d}S}{\mathrm{d}t} = k \frac{\partial T_s}{\partial r} - \frac{\partial T_l}{\partial r},$$
$$\text{and} \quad (1 - \epsilon \hat{\alpha}) c_l \frac{\mathrm{d}S}{\mathrm{d}t} = \epsilon^2 \hat{D} \frac{\partial c_s}{\partial r} - \epsilon \frac{\partial c_l}{\partial r}, \quad \text{at } s = S(t), \tag{2.2c}$$

$$\frac{\partial c_l}{\partial r} = 0 \quad \text{and} \quad \frac{\partial T_l}{\partial r} = 0 \quad \text{at } r = 0, \quad \frac{\partial c_s}{\partial r} = 0 \quad \text{and} \quad T_s = -1 \quad \text{at } r = 1, \tag{2.2d}$$

$$c_l = \epsilon \hat{c}_0, \quad T_l = \epsilon \hat{T}_0, \quad \text{and} \quad S = 1, \quad \text{at} \quad t = 0. \tag{2.2e}$$

In order to solve (2.2), we shall employ the method at matched asymptotics. When we take the large Lewis number limit, we identify three different time regimes in the problem, and within each regime there are different spatial layers. Overall, we identify the eight layers, as shown in Figure 2. When we then take the small Stefan number limit, we need to consider five extra layers within regime i, which are studied in Section 4. Once solutions are obtained in each layer, we then match them in order to obtain the asymptotic solution for the whole problem. Notice that we use hats for the position of the interface and the temperature and concentration profiles whenever they are rescaled with powers of ϵ. On the other hand, we use tildes when a variable is rescaled with powers of St, regardless of whether it has been previously rescaled with powers of ϵ or not. To minimise confusion, we give a reminder of the rescalings at the beginning of the analysis of each layer.

Similarly to the analysis in [4], the scalings in Figure 2 are primarily picked by the physics. At the start of the process, which is regime i, we expect to see diffusion of both heat and impurities, but, given the difference in the size of the diffusion coefficients, we need to introduce an inner layer of size $\mathcal{O}(\epsilon)$ around the interface (named layer B) to capture the rejection and transport of impurities, while heat diffusion is observed in the outer layers (A and C). Contrary to what we observed in the planar problem, now the interfacial concentration does not remain constant at leading order, and therefore, the solutions in regime i cease to hold when the interfacial concentration increases to $c_i = \mathcal{O}\left(\epsilon^{-1}\right)$, which occurs when $S = \mathcal{O}\left(\epsilon^{1/3}\right)$. This motivates the introduction of regime ii, in which we need to distinguish three layers: an outer layer D in the solid phase where temperature and concentration remain constant, an intermediate layer E of size $\mathcal{O}\left(\epsilon^{1/3}\right)$ near the origin in which we observe the motion of the solidification front (and which, using the Stefan condition, provides the timescale of this regime) and an inner layer F around the moving boundary where we observe rejection and transport of impurities, similar to what we previously observed in layer B. At the end of this regime, we have that the position of the interface becomes zero at leading order, and therefore, the liquid part of layer E vanishes, so the inner layer F notices the symmetry condition at $r = 0$. Hence, we need to introduce regime iii, in which the scalings are motivated by the diffusion of impurities in the liquid phase. These scalings reveal two layers: an outer layer G in the solid phase where temperature and concentration remain constant, and an inner layer H near the origin where we observe diffusion of impurities in the liquid phase and the motion of the solidification front.

We observe that in regimes ii and iii, the interfacial concentration is of size $c_i = \mathcal{O}\left(\epsilon^{-1}\right)$, which is not realistic. We notice as well that the model predicts that the solidification process never finishes, contradicting the experimental observations. Therefore, similar to what happened

https://doi.org/10.1017/S095679252000011X Published online by Cambridge University Press

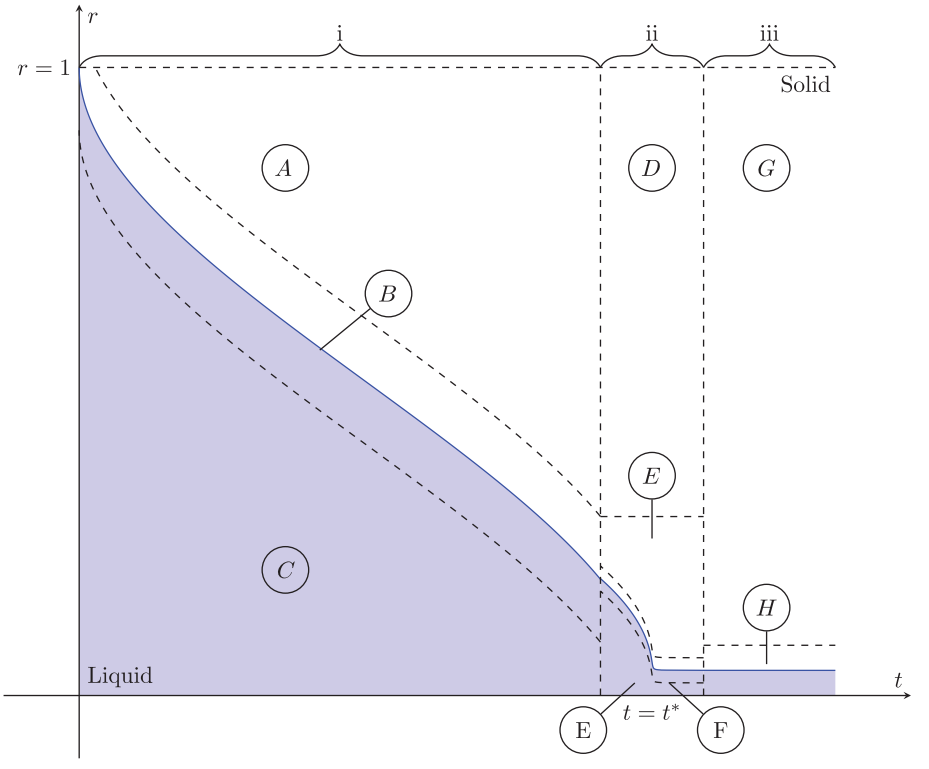

		t	r	S	c_s	c_l	T_s	T_l
Regime i	A	t	r	S	$\epsilon\hat{c}_s$	–	T_s	–
	B	t	$S(t)+\epsilon R$	S	$\epsilon\hat{c}_s$	c_l	$\epsilon\hat{T}_s$	$\epsilon\hat{T}_l$
	C	t	r	S	–	$\epsilon\hat{c}_l$	–	$\epsilon\hat{T}_l$
Regime ii	D	$t^*+\epsilon^{\frac{2}{3}}\tau$	r	$\epsilon^{\frac{1}{3}}\hat{S}$	$\epsilon\hat{c}_s$	–	T_s	–
	E	$t^*+\epsilon^{\frac{2}{3}}\tau$	$\epsilon^{\frac{1}{3}}\xi$	$\epsilon^{\frac{1}{3}}\hat{S}$	c_s	$\epsilon\hat{c}_l$	T_s	T_l
	F	$t^*+\epsilon^{\frac{2}{3}}\tau$	$\epsilon^{\frac{1}{3}}\left(\hat{S}(\tau)+\epsilon R\right)$	$\epsilon^{\frac{1}{3}}\hat{S}$	c_s	$\epsilon^{-1}\hat{c}_l$	T_s	T_l
Regime iii	G	$t^*+\epsilon^{\frac{1}{3}}\theta$	r	$\epsilon^{\frac{2}{3}}\hat{S}$	$\epsilon\hat{c}_s$	–	T_s	–
	H	$t^*+\epsilon^{\frac{1}{3}}\theta$	$\epsilon^{\frac{2}{3}}R$	$\epsilon^{\frac{2}{3}}\hat{S}$	c_s	$\epsilon^{-1}\hat{c}_l$	T_s	T_l

FIGURE 2. Sketch of the regimes and layers in the process and table of scalings for the variables in each layer of the problem. The sketch shows the evolution of the interface $S(t)$ in time, so the area above (in white) is the solid and the area below (in blue) is the liquid. The three regimes, identified with lower case Roman numerals, are the behaviours at different times. In each regime, we consider various layers which are labelled with letters. The variables τ and θ represent time at different scalings, and the variables ξ and R are the space variables in the intermediate and inner layers of each regime, respectively. For the position of the interface, temperature and concentration, we use hats whenever they are rescaled.

https://doi.org/10.1017/S095679252000011X Published online by Cambridge University Press

for the planar problem in [4], we find that in regimes ii and iii, the model loses some physical relevance as some of the modelling assumptions no longer hold, but it still has interest from the mathematical point of view as it provides a full picture of (2.2).

In the following sections, we determine asymptotic solutions in each layer and then match them to construct solutions valid over the whole problem domain.

3 Asymptotic solutions in regime i

We start by considering the behaviour at the beginning of the process, described in regime i. In this regime, the interface is far from the centre, and we distinguish three space layers: the outer layer, A, in the solid; the inner layer, B, around the moving interface which comprises both phases; and the outer layer, C, in the liquid. We solve the equations for each layer and then proceed to match the layers between them in order to fully determine the solutions.

3.1 Layer A

The first layer in this regime is the outer layer in the solid phase: layer A. Rescaling the problem using the scalings in Figure 2, which for this layer is only $c_s = \epsilon \hat{c}_s$, we find that the problem is defined by

$$\frac{\partial \hat{c}_s}{\partial t} = \epsilon^2 \hat{D}\left(\frac{\partial^2 \hat{c}_s}{\partial r^2} + \frac{2}{r}\frac{\partial \hat{c}_s}{\partial r}\right), \quad \frac{\partial T_s}{\partial t} = \kappa\left(\frac{\partial^2 T_s}{\partial r^2} + \frac{2}{r}\frac{\partial T_s}{\partial r}\right), \quad \text{in } S(t) < r < 1, \tag{3.1a}$$

$$\frac{\partial \hat{c}_s}{\partial r} = 0, \quad T_s = -1, \quad \text{at } r = 1, \tag{3.1b}$$

and, as initially all the material is liquid, we have no additional initial conditions. The problem is completed with the corresponding matching conditions which are discussed in Section 3.4. Expanding $\hat{c}_s = \hat{c}_{s0} + \epsilon \hat{c}_{s1} + \mathcal{O}\left(\epsilon^2\right)$ and $T_s = T_{s0} + \epsilon T_{s1} + \mathcal{O}\left(\epsilon^2\right)$, we find that at leading order

$$\hat{c}_{s0} = \hat{\alpha} c_i\left(S_0^{-1}(r)\right) = \hat{\alpha}\frac{\hat{c}_0}{3}\frac{k\mathrm{St}}{\rho}\frac{1-r^3}{(1-r)r^3}, \tag{3.2}$$

where c_i is the concentration at the interface as defined in Section 3.4; while T_{s0} is the solution to the problem

$$\frac{\partial T_{s0}}{\partial t} = \kappa\left(\frac{\partial^2 T_{s0}}{\partial r^2} + \frac{2}{r}\frac{\partial T_{s0}}{\partial r}\right), \quad \text{for } S_0(t) < r < 1, \tag{3.3a}$$

$$T_{s0} = 0 \quad \text{at } r = S_0(t), \quad \text{and} \quad T_{s0} = -1 \quad \text{at } r = 1, \tag{3.3b}$$

$$\frac{\rho}{\mathrm{St}}\frac{\mathrm{d}S_0}{\mathrm{d}t} = k\frac{\partial T_{s0}}{\partial r} \quad \text{at } r = S_0(t), \quad \text{and} \quad S_0 = 1 \quad \text{at } t = 0, \tag{3.3c}$$

with the latter condition derived from matching in Section 3.4.

Notice that this problem corresponds to the one-phase Stefan problem, and so, within this regime, we need to distinguish different timescales, as discussed in [30, 37]. We give the analysis of these different timescales in Section 4.

https://doi.org/10.1017/S095679252000011X Published online by Cambridge University Press

3.2 Layer *B*

Layer B is the inner layer of size ϵ around the moving interface. Therefore, defining the inner variable $R = \frac{r-S(t)}{\epsilon}$, and using the scalings $c_s = \epsilon \hat{c}_s$, $T_s = \epsilon \hat{T}_s$, $T_l = \epsilon \hat{T}_l$, we find that the problem is defined as

$$\epsilon \frac{\partial \hat{c}_s}{\partial t} = S'(t)\frac{\partial \hat{c}_s}{\partial R} + \epsilon \hat{D}\left(\frac{\partial^2 \hat{c}_s}{\partial R^2} + \epsilon \frac{2}{S(t)+\epsilon R}\frac{\partial \hat{c}_s}{\partial R}\right), \tag{3.4a}$$

$$\epsilon^2 \frac{\partial \hat{T}_s}{\partial t} = \epsilon S'(t)\frac{\partial \hat{T}_s}{\partial R} + \kappa\left(\frac{\partial^2 \hat{T}_s}{\partial R^2} + \epsilon \frac{2}{S(t)+\epsilon R}\frac{\partial \hat{T}_s}{\partial R}\right), \tag{3.4b}$$

for $R > 0$, and

$$\epsilon \frac{\partial c_l}{\partial t} = S'(t)\frac{\partial c_l}{\partial R} + \frac{\partial^2 c_l}{\partial R^2} + \epsilon \frac{2}{S(t)+\epsilon R}\frac{\partial c_l}{\partial R}, \tag{3.4c}$$

$$\epsilon^2 \frac{\partial \hat{T}_l}{\partial t} = \epsilon S'(t)\frac{\partial \hat{T}_l}{\partial R} + \frac{\partial^2 \hat{T}_l}{\partial Z^2} + \epsilon \frac{2}{S(t)+\epsilon R}\frac{\partial \hat{T}_l}{\partial R}, \tag{3.4d}$$

for $R < 0$. At the interface, $R = 0$, we have

$$\hat{T}_s = \hat{T}_l, \quad \hat{c}_s = \hat{\alpha} c_l, \quad c_l = -\hat{m}_l \hat{T}_l, \quad \frac{\rho}{\mathrm{St}}\frac{\mathrm{d}S}{\mathrm{d}t} = k\frac{\partial \hat{T}_s}{\partial R} - \frac{\partial \hat{T}_l}{\partial R},$$
$$\text{and} \quad (1-\epsilon\hat{\alpha})c_l \frac{\mathrm{d}S}{\mathrm{d}t} = \epsilon^2 \hat{D}\frac{\partial \hat{c}_s}{\partial R} - \frac{\partial c_l}{\partial R}. \tag{3.4e}$$

The remaining conditions are given by the matching conditions with layers A and C. The solutions are found to be

$$c_s = \epsilon \hat{\alpha} c_i(t) + \mathcal{O}\left(\epsilon^2\right), \tag{3.5a}$$

$$c_l = c_i(t)e^{-S_0'(t)R} + \epsilon\left(\mathcal{A}_1(t) + \mathcal{A}_2(t,R)e^{-S_0'(t)R}\right) + \mathcal{O}\left(\epsilon^2\right), \tag{3.5b}$$

$$T_s = \epsilon\left(A_1(t)R - \frac{c_i(t)}{\hat{m}_l}\right) + \mathcal{O}\left(\epsilon^2\right), \tag{3.5c}$$

$$T_l = \epsilon\left(\left(kA_1(t) - \frac{\rho}{\mathrm{St}}S_0'(t)\right)R - \frac{c_i(t)}{\hat{m}_l}\right) + \mathcal{O}\left(\epsilon^2\right), \tag{3.5d}$$

where

$$\mathcal{A}_1(t) = \frac{c_i'(t)}{S_0'(t)^2} + c_i(t)\left(\hat{\alpha} + \frac{2}{S_0(t)S_0'(t)} - \frac{S_0''(t)}{S_0'(t)^3}\right), \tag{3.6a}$$

$$\mathcal{A}_2(t,R) = -\frac{c_i'(t)}{S_0'(t)^2}\left(1 + S_0'(t)R\right) + A_2(t)$$
$$+ c_i(t)\left[\frac{S_0''(t)}{S_0'(t)^3}\left(1 + S_0'(t)R + \frac{1}{2}S_0'(t)^2R^2\right) - \frac{\left(1+S_0'(t)R\right)\left(2+S_0(t)S_1'(t)\right)}{S_0'(t)S_0(t)}\right], \tag{3.6b}$$

https://doi.org/10.1017/S095679252000011X Published online by Cambridge University Press

while $c_i(t)$, $A_1(t)$ and $A_2(t)$ are functions to be determined from the matching. Matching c_l from layers A to B, we obtain

$$c_i'(t) + c_i(t)\left(\hat{\alpha}S_0'(t)^2 + 2\frac{S_0'(t)}{S_0(t)} - \frac{S_0''(t)}{S_0'(t)}\right) = \hat{c}_0 S_0'(t)^2, \tag{3.7}$$

which allows us to determine $c_i(t)$ once we know $S_0(t)$. We give the calculations for $c_i(t)$ in Section 4.

3.3 Layer *C*

The last layer in regime i is layer C, the outer layer in the liquid. Rescaling the problem with $c_l = \epsilon\hat{c}_l$ and $T_l = \epsilon\hat{T}_l$, we find that the problem is defined in $0 < r < S(t)$ by

$$\frac{\partial \hat{c}_l}{\partial t} = \epsilon\left(\frac{\partial^2 \hat{c}_l}{\partial r^2} + \frac{2}{r}\frac{\partial \hat{c}_l}{\partial r}\right), \quad \frac{\partial \hat{T}_l}{\partial t} = \frac{\partial^2 \hat{T}_l}{\partial r^2} + \frac{2}{r}\frac{\partial \hat{T}_l}{\partial r}, \quad \text{in } 0 < r < S(t), \tag{3.8a}$$

$$\frac{\partial \hat{c}_l}{\partial r} = 0 \quad \text{and} \quad \frac{\partial \hat{T}_l}{\partial r} = 0, \quad \text{at } r = 0, \quad \text{and} \quad \hat{c}_l = \hat{c}_0 \quad \text{and} \quad \hat{T}_l = \hat{T}_0, \quad \text{at } t = 0. \tag{3.8b}$$

The problem is completed by the matching conditions with layer B. The leading-order solutions are $c_l = \epsilon\hat{c}_0$, $T_l = \epsilon\hat{T}_{l0}(t, r)$, where the problem for $\hat{T}_{l0}$ is given by

$$\frac{\partial \hat{T}_{l0}}{\partial t} = \frac{\partial^2 \hat{T}_{l0}}{\partial r^2} + \frac{2}{r}\frac{\partial \hat{T}_{l0}}{\partial r}, \quad \text{for } 0 < r < S_0(t), \tag{3.9a}$$

$$\frac{\partial \hat{T}_{l0}}{\partial r} = 0 \quad \text{at } r = 0, \quad \hat{T}_{l0} = -\frac{c_i(t)}{\hat{m}_l} \quad \text{at } r = S_0(t), \quad \text{and} \quad \hat{T}_{l0} = \hat{T}_0 \quad \text{at } t = 0, \tag{3.9b}$$

where the latter two conditions in (3.9b) are derived in Section 3.4. We solve (3.9) in Section 4.

3.4 Matching of the solutions

We can now match the solutions between the different layers using Van Dyke's rule (see [42] for details). The notation we use to denote the asymptotic expansions is the following. By ($m$ti)($n$to), we mean taking n terms in the outer solution written in terms of the inner variable and expanded to mth order in the inner variable. Similarly, by ($n$to)($m$ti), we mean taking m terms in the inner solution written in terms of the outer variable and expanded to nth order in the outer variable. Then, according to Van Dyke's rule, these two expansions have to be equal for any n and m.

We start matching c_l between the outer layer C and the inner layer B. We take two terms in the inner solution and two terms in the outer solution and write them both in terms of the inner variable, so $\epsilon\hat{c}_0 = (2\text{ti})(2\text{to}) = (2\text{to})(2\text{ti}) = \epsilon\mathcal{A}_1(t)$, and therefore, we have

$$\frac{c_i'(t)}{S_0'(t)^2} + c_i(t)\left(\hat{\alpha} + \frac{2}{S_0(t)S_0'(t)} - \frac{S_0''(t)}{S_0'(t)^3}\right) = \hat{c}_0, \tag{3.10}$$

which is the equation (3.7) we have used to determine $c_i(t)$ at leading order.

We next match c_s between the outer layer A and the inner layer B though $\epsilon\hat{c}_{s0}(S_0(t)) = (2\text{ti})(2\text{to}) = (2\text{to})(2\text{ti}) = \epsilon\hat{\alpha}c_i(t)$, giving $\hat{c}_{s0}(S_0(t)) = \hat{\alpha}c_i(t)$, and so we can conclude that $\hat{c}_{s0}(r)$ is $\hat{c}_{s0}(r) = \hat{\alpha}c_i\left(S_0^{-1}(r)\right)$.

https://doi.org/10.1017/S095679252000011X Published online by Cambridge University Press

We now match the temperature in the solid phase, T_s, between layers A and B. Taking two terms in the inner solution and two terms in the outer solution, and writing them in terms of the inner variable, (2ti)(2to) = (2to)(2ti). We find

$$T_{s0}(t, S_0(t)) + \epsilon \left(T_{s1}(t, S_0(t)) + (R + S_1(t)) \left. \frac{\partial T_{s0}}{\partial r} \right|_{r=S_0(t)} \right) = \epsilon \left(A_1(t) R - \frac{c_i(t)}{\hat{m}_l} \right), \tag{3.11}$$

from which we conclude

$$A_1(t) = \left. \frac{\partial T_{s0}}{\partial r} \right|_{r=S_0(t)} \quad \text{and} \quad T_{s0}(t, S_0(t)) = 0. \tag{3.12}$$

We use the latter as a boundary condition to complete (3.3).

Finally, we match the temperature in the liquid phase between layers B and C. Taking two terms in both the inner and outer solutions, and writing them in terms of the inner variable, we find

$$\epsilon \hat{T}_{l0}(t, S_0(t)) = (2\text{ti})(2\text{to}) = (2\text{to})(2\text{ti}) = \epsilon \left(\left(k A_1(t) - \frac{\rho}{\text{St}} S_0'(t) \right) R - \frac{c_i(t)}{\hat{m}_l} \right), \tag{3.13}$$

which give the boundary condition we need for (3.9)

$$\hat{T}_{l0}(t, S_0(t)) = -\frac{c_i(t)}{\hat{m}_l}, \tag{3.14}$$

and the condition for the moving boundary,

$$\frac{\rho}{\text{St}} S_0'(t) = k \left. \frac{\partial T_{s0}}{\partial r} \right|_{r=S_0(t)}. \tag{3.15}$$

This completes the problem in this regime. In the next section, we perform an asymptotic analysis in the limit $\text{St} \to 0$ in order to find approximate solutions for regime i.

4 Small St analysis of regime i

In this section, we perform the small Stefan number analysis of the thermal problem found in the previous section. Taking the limit $\text{St} \to 0$, we can determine approximate analytical solutions to the problem in regime i. Because the concentration problem has almost decoupled from the thermal problem when taking the limit $\epsilon \to 0$, the problem we have to solve is very similar to the one studied in [30]. Still, there are three main differences between the problem in [30] and the problem studied here. The first difference is the scalings we took for the non-dimensionalisation and thus where the dimensionless parameters appear in the solutions. The second difference is that we consider constitutional supercooling, therefore the temperature at the interface depends on the concentration of impurities at the interface which is found from an ordinary differential equation that depends on the position of the interface, but not on the temperature. The last difference is that in our problem we have assumed that the scaled initial temperature of the melt is small, which physically means that the initial temperature is above but close to the melting temperature. The amount of supercooling is also assumed to be small. Therefore, we find that the temperature gradient in the liquid will have no influence on the position of the interface at leading order, reducing the free boundary problem to a one-phase Stefan problem.

https://doi.org/10.1017/S095679252000011X Published online by Cambridge University Press

This last assumption is crucial to decouple the thermal problem into the following subproblems.

The first subproblem is a one-phase Stefan problem, involving temperature in the solid phase and the moving boundary given by (3.3). Once we have solved problem (3.3), we can use $S_0(t)$ to calculate the concentration at the interface from (3.7). Finally, knowing the concentration at the interface, we can solve the problem for the temperature in the liquid given in (3.9).

To solve these problems, we follow the same method as in [30], finding asymptotic solutions in the limit $\mathrm{St} \to 0$. Therefore, within regime i, we need to distinguish five different sublayers which now scale with St. These five new sublayers are showed in red in Figure 3. Notice that to avoid confusion with rescalings with ϵ, we use tilde to denote the rescalings with St.

4.1 Subregime i(1)

The first subregime we have to study is subregime i(1) which corresponds to early time. In this layer $t = \mathcal{O}(1)$, which is small compared to the critical time $t^* = \mathcal{O}(\mathrm{St}^{-1})$. This critical time corresponds to the solidification time of the equivalent pure melt problem. In this layer, the interface has not moved much, so it is near $r = 1$, and we can write it as $S_0 = 1 + \sqrt{\mathrm{St}}\tilde{S}_0$. Therefore, we need to consider an outer layer in the liquid phase and an inner layer comprising both phases defined as $r = 1 + \sqrt{\mathrm{St}}R$, where R is the inner variable.

4.1.1 *Layer* a

We first focus on the outer solution in the liquid phase. The thermal problem in the liquid is

$$\frac{\partial \hat{T}_{l0}}{\partial t} = \frac{\partial^2 \hat{T}_{l0}}{\partial r^2} + \frac{2}{r}\frac{\partial \hat{T}_{l0}}{\partial r}, \quad \text{for } 0 < r < 1, \tag{4.1a}$$

$$\frac{\partial \hat{T}_{l0}}{\partial r} = 0 \ \text{ at } r = 0, \quad \hat{T}_{l0} = 0 \ \text{ at } \ r = 1, \quad \hat{T}_{l0} = \hat{T}_0 \ \text{ at } t = 0, \tag{4.1b}$$

where the condition at $r = 1$ comes from the matching conditions with layer b. Using separation of variables, we find that the solution at leading order is [30]

$$\hat{T}_{l0} = \frac{2\hat{T}_0}{\pi r}\sum_{n=1}^{\infty}\frac{(-1)^{n+1}}{n}e^{-n^2\pi^2 t}\sin(n\pi r) + \mathcal{O}\left(\sqrt{\mathrm{St}}\right). \tag{4.2}$$

4.1.2 *Layer* b

We now solve the system in the inner layer b. This layer accounts for both the solid and liquid phases, therefore we need to solve for both thermal fields and the concentration at the interface. We start by solving the one-phase Stefan problem that determines the temperature in the solid and the position of the interface. With the rescalings $r = 1 + \sqrt{\mathrm{St}}R$, $S_0 = 1 + \sqrt{\mathrm{St}}\tilde{S}_0$, $\hat{T}_{l0} = \sqrt{\mathrm{St}}\tilde{T}_{l0}$ and $c_i = \epsilon\tilde{c}_i$, the problem (3.3) becomes

$$\mathrm{St}\frac{\partial T_{s0}}{\partial t} = \kappa\left(\frac{\partial^2 T_{s0}}{\partial R^2} + \frac{2\sqrt{\mathrm{St}}}{1 + \sqrt{\mathrm{St}}R}\frac{\partial T_{s0}}{\partial R}\right), \quad \text{for } \tilde{S}_0(t) < R < 0, \tag{4.3a}$$

$$T_{s0} = 0 \ \text{ at } R = \tilde{S}_0(t), \tag{4.3b}$$

https://doi.org/10.1017/S095679252000011X Published online by Cambridge University Press

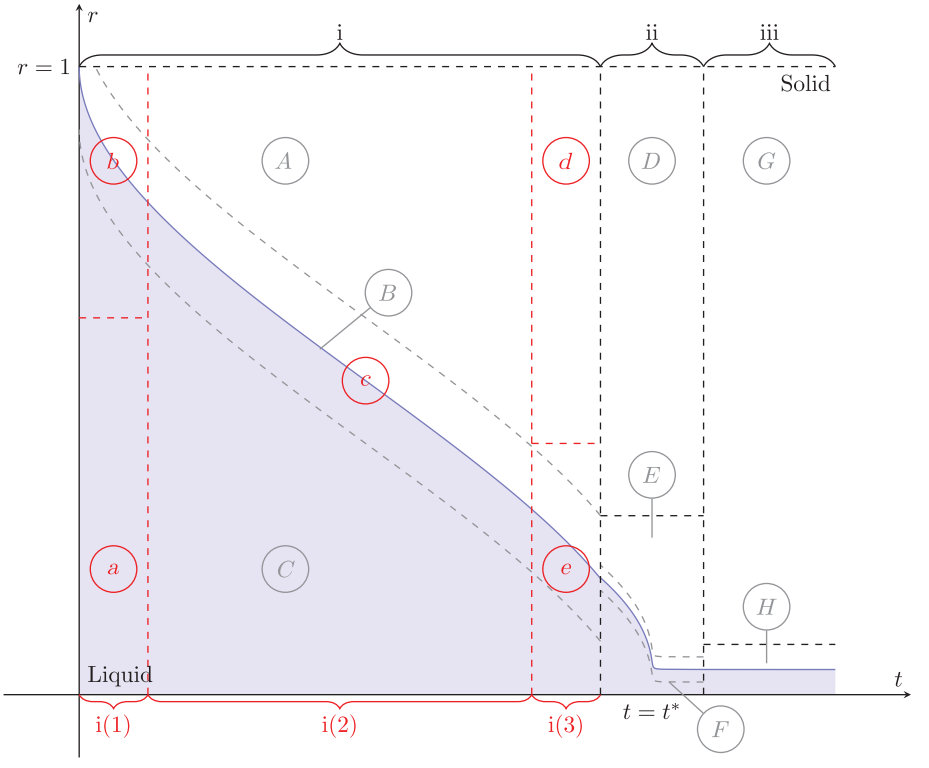

		t	r	S_0	T_{s0}	$\hat{T}_{l0}$	c_i
Subregime i(a)	a	t	r	$1+\sqrt{\mathrm{St}}\tilde{S}_0$	–	$\hat{T}_{l0}$	$\mathrm{St}\tilde{c}_i$
	b	t	$1+\sqrt{\mathrm{St}}R$	$1+\sqrt{\mathrm{St}}\tilde{S}_0$	T_{s0}	$\sqrt{\mathrm{St}}\tilde{T}_{l0}$	$\mathrm{St}\tilde{c}_i$
Subregime i(2)	c	$\mathrm{St}^{-1}\tilde{t}$	r	S_0	T_{s0}	$\hat{T}_{l0}$	$\mathrm{St}\tilde{c}_i$
Subregime i(3)	d	$t^*+\tilde{t}$	r	$\sqrt{\mathrm{St}}\tilde{S}_0$	T_{s0}	–	$\mathrm{St}^{-\frac{1}{2}}\tilde{c}_i$
	e	$t^*+\tilde{t}$	$\sqrt{\mathrm{St}}R$	$\sqrt{\mathrm{St}}\tilde{S}_0$	T_{s0}	$\mathrm{St}^{-\frac{1}{2}}\tilde{T}_{l0}$	$\mathrm{St}^{-\frac{1}{2}}\tilde{c}_i$

FIGURE 3. Sketch of the layers in St in regime i and table of scalings for the variables in each sublayer of regime i. The new layers are shown on top of the layers in ϵ discussed in Figure 2, and they are identified with lower case letters. The subregimes within regime i are identified as subregimes i(1), i(2) and i(3). The variable R is the space variable in the inner layers. For temperature, concentration and time, we use tildes whenever they are rescaled with powers of St.

$$T_{s0} = -1 \quad \text{at } R = 0, \tag{4.3c}$$

$$\rho \frac{\mathrm{d}\tilde{S}_0}{\mathrm{d}t} = k \frac{\partial T_{s0}}{\partial R} \quad \text{at } R = \tilde{S}_0(t), \tag{4.3d}$$

$$\tilde{S}_0 = 0, \qquad \text{at } t = 0. \tag{4.3e}$$

https://doi.org/10.1017/S095679252000011X Published online by Cambridge University Press

Expanding T_{s0} and $\tilde{S}_0$ in powers of $\sqrt{\text{St}}$, we find

$$T_{s0} = \frac{R}{\tilde{S}_{0,0}(t)} - 1 + \sqrt{\text{St}}\left(-\frac{R^2}{\tilde{S}_{0,0}(t)} + \left(1 - \frac{\tilde{S}_{0,1}(t)}{\tilde{S}_{0,0}(t)^2}\right)R\right) + \mathcal{O}(\text{St}), \tag{4.4a}$$

$$\tilde{S}_0 = -\sqrt{\frac{2k}{\rho}t} - \sqrt{\text{St}}\frac{2k}{3\rho}t + \mathcal{O}(\text{St}). \tag{4.4b}$$

We now need to determine $\tilde{c}_i$ using the calculated values of $\tilde{S}_0$. With the rescaled concentration, (3.7) becomes

$$\tilde{c}_i'(t) + \tilde{c}_i(t)\left(\text{St}\hat{\alpha}\tilde{S}_0'(t)^2 + 2\sqrt{\text{St}}\frac{\tilde{S}_0'(t)}{1+\sqrt{\text{St}}\tilde{S}_0(t)} - \frac{\tilde{S}_0''(t)}{\tilde{S}_0'(t)}\right) = \hat{c}_0\tilde{S}_0'(t)^2, \tag{4.5}$$

and expanding $\tilde{c}_i(t)$ in powers of $\sqrt{\text{St}}$, we find

$$\tilde{c}_i = \frac{\hat{c}_0 k}{\rho} + \sqrt{\text{St}}\hat{c}_0\sqrt{\left(\frac{2k}{\rho}\right)^3 t} + \mathcal{O}(\text{St}), \tag{4.6}$$

where we have used the fact that we require $\tilde{c}_i$ to remain bounded as $t \to 0$ as our initial condition.

Finally, we can use the values of $\tilde{c}_i$ and $\tilde{S}_0$ to determine the temperature in the liquid. Rescaling (3.9), we have

$$\text{St}\frac{\partial \tilde{T}_{l0}}{\partial t} = \frac{\partial^2 \tilde{T}_{l0}}{\partial R^2} + \frac{2\sqrt{\text{St}}}{1+\sqrt{\text{St}}R}\frac{\partial \tilde{T}_{l0}}{\partial R}, \quad \text{in} \quad R < \tilde{S}_0(t), \tag{4.7a}$$

$$\tilde{T}_{l0} = -\frac{\tilde{c}_i(t)}{\hat{m}_l} \quad \text{at} \quad R = \tilde{S}_0(t), \tag{4.7b}$$

and the remaining condition is given by the matching with the outer layer. Then, in the inner layer, the temperature is given by

$$\tilde{T}_{l0} = -2\hat{T}_0 R\sum_{n=1}^{\infty} e^{-n^2\pi^2 t}\left(R - \hat{S}_{0,0}(t)\right)\sqrt{\text{St}} + \mathcal{O}(\text{St}). \tag{4.8}$$

Notice that the supercooling effects are of $\mathcal{O}(\text{St})$, therefore they are only seen at higher order.

Then, the solution to the problem in this subregime is given, at leading order, by

$$T_{s0} \approx -1 + \sqrt{\frac{\rho}{2k\text{St}}}\frac{1-r}{\sqrt{t}}, \tag{4.9a}$$

$$\hat{T}_{l0} \approx \frac{2\hat{T}_0}{\pi r}\sum_{n=1}^{\infty}\frac{(-1)^{n+1}}{n}e^{-n^2\pi^2 t}\sin(n\pi r), \tag{4.9b}$$

$$S_0 \approx 1 - \sqrt{\frac{2k\text{St}}{\rho}t}, \tag{4.9c}$$

$$c_i \approx \hat{c}_0\frac{k\text{St}}{\rho}. \tag{4.9d}$$

https://doi.org/10.1017/S095679252000011X Published online by Cambridge University Press

4.2 Subregime i(2) (layer c)

Now we need to consider the central subregime i(2), in which $t = \mathcal{O}(\mathrm{St}^{-1})$. For this problem, we only need to consider one layer. We start solving the one-phase Stefan problem (3.3) which, with the new time scaling $t = \mathrm{St}^{-1}\tilde{t}$, becomes

$$\mathrm{St}\frac{\partial T_{s0}}{\partial \tilde{t}} = \kappa\left(\frac{\partial^2 T_{s0}}{\partial r^2} + \frac{2}{r}\frac{\partial T_{s0}}{\partial r}\right), \quad \text{in} \quad S_0(\tilde{t}) < r < 1, \tag{4.10a}$$

$$T_{s0} = 0, \quad \text{at } r = S_0(\tilde{t}), \quad T_{s0} = -1, \quad \text{at} \quad r = 1, \quad \rho\frac{\mathrm{d}S_0}{\mathrm{d}\tilde{t}} = k\frac{\partial T_{s0}}{\partial r} \quad \text{at} \quad r = S_0(\tilde{t}), \tag{4.10b}$$

and the initial conditions come from matching with subregime i(1). For convenience, as done in [30], we take r and S_0 to be the independent variables, so then the dependent variables are $T_{s0}(S_0, r)$ and $\tilde{t}(S_0)$. Then, we expand T_{s0} and $\tilde{t}$ as

$$T_{s0} = \frac{1}{1-S_0}\left(\frac{S_0}{r} - 1\right) + \mathrm{St}\frac{k}{\kappa\rho}\frac{1-r}{6rS_0(1-S_0)}\left(1 - \left(\frac{1-r}{1-S_0}\right)^2\right) + \mathcal{O}\left(\mathrm{St}^2\right), \tag{4.11a}$$

$$\tilde{t} = \frac{\rho}{k}\left(\frac{1}{2}(1-S_0)^2 - \frac{1}{3}(1-S_0)^3\right) + \mathrm{St}\frac{1}{6\kappa}(1-S_0)^2 + \mathcal{O}\left(\mathrm{St}^2\right). \tag{4.11b}$$

Notice that when $S_0^2 = \mathcal{O}(\mathrm{St})$, this solution breaks down, so this motivates the study of subregime i(3). Now, we need to determine the concentration at the interface from (3.7), which, rescaling time and the concentration itself as $c_i = \mathrm{St}\tilde{c}_i$, becomes

$$\tilde{c}_i'(\tilde{t}) = \hat{c}_0 S_0'(\tilde{t})^2 - \tilde{c}_i(\tilde{t})\left(\mathrm{St}\hat{\alpha}S_0'(\tilde{t})^2 + 2\frac{S_0'(\tilde{t})}{S_0(\tilde{t})} - \frac{S_0''(\tilde{t})}{S_0'(\tilde{t})}\right). \tag{4.12}$$

As we did before, we take S_0 to be the time-like independent variable and $\hat{t}$ the dependent variable. Then, we rewrite (4.12) as

$$\tilde{c}_i'(S_0)\tilde{t}'(S_0) = \hat{c}_0 - \tilde{c}_i(S_0)\left(\mathrm{St}\hat{\alpha} + \frac{2}{S_0}\tilde{t}'(S_0) + \tilde{t}''(S_0)\right). \tag{4.13}$$

Expanding $\tilde{c}_i(\tilde{t})$ and $\tilde{t}$ in powers of St, we find that, at leading order,

$$\tilde{c}_{i,0}'(S_0)\tilde{t}_{,0}'(S_0) = \hat{c}_0 - \tilde{c}_{i,0}(S_0)\left(\frac{2}{S_0}\tilde{t}_{,0}'(S_0) + \tilde{t}_{,0}''(S_0)\right), \tag{4.14}$$

therefore, using the definition of $\tilde{t}_{,0}(S_0)$ from (4.11b), we find

$$\tilde{c}_{i,0}(S_0) = \frac{3C_1\rho - \hat{c}_0 k S_0^3}{3\rho(1-S_0)S_0^3}, \tag{4.15}$$

where C_1 is a constant to be determined. Matching with the solution in subregime i(1), we find $C_1 = \frac{\hat{c}_0 k}{3\rho}$, therefore we conclude that

$$\tilde{c}_{i,0} = \frac{\hat{c}_0}{3}\frac{k}{\rho}\frac{1-S_0^3}{(1-S_0)S_0^3}. \tag{4.16}$$

Note that we could alternatively determine the value of C_1 by imposing that $\tilde{c}_i$ is bounded as $S_0 \to 1$, finding the same result.

https://doi.org/10.1017/S095679252000011X Published online by Cambridge University Press

Finally, we need to determine the temperature in the liquid from the rescaled version of (3.9), which is

$$\mathrm{St}\frac{\partial \hat{T}_{l0}}{\partial \hat{t}} = \frac{\partial^2 \hat{T}_{l0}}{\partial r^2} + \frac{2}{r}\frac{\partial \hat{T}_{l0}}{\partial r}, \quad \text{in} \quad 0 < r < S_0(\tilde{t}), \tag{4.17a}$$

$$\frac{\partial \hat{T}_{l0}}{\partial r} = 0 \quad \text{at} \quad r = 0, \quad \hat{T}_{l0} = -\mathrm{St}\frac{\tilde{c}_i(\hat{t})}{\hat{m}_l} \quad \text{at} \quad r = S_0(\tilde{t}), \tag{4.17b}$$

and the initial conditions from the matching with regime i(1).

In order to solve this problem, we proceed as in [30], and however, we need to introduce extra terms in powers of St to account for the non-homogeneous boundary condition. We find that the solution to leading order is given by

$$\hat{T}_{l0} = \frac{2\hat{T}_0 S_0(\tilde{t})}{\pi r}\sum_{n=1}^{\infty}\frac{(-1)^{n+1}}{n}\exp\left(-\frac{n^2\pi^2}{\mathrm{St}}\int_0^{\tilde{t}}\frac{\mathrm{d}\tilde{s}}{S_0(\tilde{s})^2}\right)\sin\left(\frac{n\pi r}{S_0(\tilde{t})}\right) - \mathrm{St}\frac{\tilde{c}_{i0}(\tilde{t})}{\hat{m}_l}. \tag{4.18}$$

Notice that, as discussed in [30], the inclusion of the exponentially small terms allows us to match the initial conditions, and thus it is not necessary to consider subregime i(1).

Then, the solution to the problem in this subregime at leading order is given by

$$T_{s0} \approx \frac{1}{1 - S_0(t)}\left(\frac{S_0(t)}{r} - 1\right), \tag{4.19a}$$

$$\hat{T}_{l0} \approx -\frac{c_i(t)}{\hat{m}_l} + \frac{2\hat{T}_0 S_0(t)}{\pi r}\sum_{n=1}^{\infty}\frac{(-1)^{n+1}}{n}\exp\left(-n^2\pi^2\int_0^{t}\frac{\mathrm{d}s}{S_0(s)^2}\right)\sin\left(\frac{n\pi r}{S_0(t)}\right), \tag{4.19b}$$

$$t \approx \frac{\rho}{k\mathrm{St}}\left(\frac{1}{2}(1 - S_0)^2 - \frac{1}{3}(1 - S_0)^3\right), \tag{4.19c}$$

$$c_i \approx \frac{\hat{c}_0}{3}\frac{k\mathrm{St}}{\rho}\frac{1 - S_0(t)^3}{(1 - S_0(t))S_0(t)^3}. \tag{4.19d}$$

The explicit form of $S_0(t)$ can be found inverting (4.19c), but for simplicity we do not reproduce the result here.

4.3 Subregime i(3)

We finally consider the last subregime, which corresponds to the late-time behaviour. This late time is $t^* - t = \mathcal{O}(1)$, where $t^* = \mathcal{O}(\mathrm{St}^{-1})$ is the critical time in which the pure material would finish solidifying. Then, we define the time variable as $t = t^* + \tilde{t}$, where $\tilde{t} < 0$ is the new time variable. In this subregime, the interface position is of $(\sqrt{\mathrm{St}})$, so we rescale $S_0 = \sqrt{\mathrm{St}}\tilde{S}_0$ and $c_i = \mathrm{St}^{-\frac{1}{2}}\tilde{c}_i$. Therefore, we need to consider an outer layer in the solid phase and an inner layer comprising both phases.

4.3.1 *Layer* d

We start by considering the outer layer in the solid phase. With the rescalings $t = t^* + \tilde{t}$, $S_0 = \sqrt{\mathrm{St}}\tilde{S}_0$ and $c_i = \mathrm{St}^{-\frac{1}{2}}\tilde{c}_i$, the system (3.3) becomes

$$\frac{\partial T_{s0}}{\partial \tilde{t}} = \kappa\left(\frac{\partial^2 T_{s0}}{\partial r^2} + \frac{2}{r}\frac{\partial T_{s0}}{\partial r}\right) \quad \text{for } 0 < r < 1, \quad T_{s0} = -1 \quad \text{at} \quad r = 1, \tag{4.20a}$$

https://doi.org/10.1017/S095679252000011X Published online by Cambridge University Press

with the corresponding matching conditions with the inner layer and the previous subregime. The latter matching gives that, at leading order, $T_{s0,0} = -1 + \mathcal{O}(\sqrt{\mathrm{St}})$, and thus we conclude that $T_{s0} \approx -1$.

4.3.2 *Layer* e

The last layer we need to study is the inner layer near the origin. The scalings in this layer are $t = t^* + \tilde{t}$, $r = \sqrt{\mathrm{St}}R$, $S_0 = \sqrt{\mathrm{St}}\tilde{S}_0$, $\hat{T}_{l0} = \mathrm{St}^{-\frac{1}{2}}\tilde{T}_{l0}$ and $c_i = \mathrm{St}^{-\frac{1}{2}}\tilde{c}_i$. We consider the one-phase Stefan problem (3.3), which once rescaled becomes

$$\mathrm{St}\frac{\partial T_{s0}}{\partial \tilde{t}} = \kappa\left(\frac{\partial^2 T_{s0}}{\partial R^2} + \frac{2}{R}\frac{\partial T_{s0}}{\partial R}\right), \quad \text{for} \quad R > \tilde{S}_0(\tilde{t}), \tag{4.21a}$$

$$T_{s0} = 0 \quad \text{at} \quad R = \tilde{S}_0(\tilde{t}), \quad \rho\frac{\mathrm{d}\tilde{S}_0}{\mathrm{d}\tilde{t}} = k\frac{\partial T_{s0}}{\partial R} \quad \text{at} \quad R = \tilde{S}_0(\tilde{t}), \tag{4.21b}$$

with matching conditions with the outer layer and the previous subregime. We find

$$T_{s0} = -1 + \frac{\tilde{S}_{0,0}(\tilde{t})}{R} + \mathcal{O}\left(\sqrt{\mathrm{St}}\right), \quad \tilde{S}_0 = \sqrt{-\frac{2k}{\rho}\tilde{t}} + \mathcal{O}\left(\sqrt{\mathrm{St}}\right). \tag{4.22}$$

We use the value of $\tilde{S}_0$ to calculate the concentration at the interface by solving

$$\tilde{c}_i'(\tilde{t}) + \tilde{c}_i(\tilde{t})\left(\mathrm{St}\hat{\alpha}\tilde{S}_0'(\tilde{t})^2 + 2\frac{\tilde{S}_0'(\tilde{t})}{\tilde{S}_0(\tilde{t})} - \frac{\tilde{S}_0''(\tilde{t})}{\tilde{S}_0'(\tilde{t})}\right) = \mathrm{St}^{\frac{3}{2}}\hat{c}_0\tilde{S}_0'(\tilde{t})^2. \tag{4.23}$$

Expanding $\tilde{c}_i$ in powers of $\sqrt{\mathrm{St}}$, we find that

$$\tilde{c}_{i,0} = \frac{\hat{c}_0}{3}\frac{k}{\rho}\frac{1}{\tilde{S}_{0,0}(\tilde{t})^3} + \mathcal{O}\left(\sqrt{\mathrm{St}}\right). \tag{4.24}$$

Finally, we determine the temperature in the liquid phase. Rescaling (3.9), we find

$$\mathrm{St}\frac{\partial \tilde{T}_{l0}}{\partial \tilde{t}} = \frac{\partial^2 \tilde{T}_{l0}}{\partial R^2} + \frac{2}{R}\frac{\partial \tilde{T}_{l0}}{\partial R}, \quad \text{for} \quad 0 < R < \tilde{S}_0(\tilde{t}), \tag{4.25a}$$

$$\frac{\partial \tilde{T}_{l0}}{\partial R} = 0 \quad \text{at} \quad R = 0, \quad \tilde{T}_{l0} = -\frac{\tilde{c}_i(\tilde{t})}{\hat{m}_l} \quad \text{at} \quad R = \tilde{S}_0(\tilde{t}), \tag{4.25b}$$

and the matching conditions with subregime i(2) act as initial conditions. Expanding the temperature in powers of $\sqrt{\mathrm{St}}$, we determine the leading-order solution as

$$\tilde{T}_{l0} = -\frac{\tilde{c}_{i,0}(\tilde{t})}{\hat{m}_l} + \mathcal{O}\left(\sqrt{\mathrm{St}}\right). \tag{4.26}$$

Then, the solution to the problem in this subregime at leading order is given by

$$T_{s0} \approx -1 + \frac{S_0(t)}{r}, \tag{4.27a}$$

$$\hat{T}_{l0} \approx -\frac{c_i(t)}{\hat{m}_l}, \tag{4.27b}$$

https://doi.org/10.1017/S095679252000011X Published online by Cambridge University Press

$$S_0 \approx \sqrt{-\frac{2k\mathrm{St}}{\rho}(t^* - t)}, \tag{4.27c}$$

$$c_i \approx \frac{\hat{c}_0}{3}\frac{k\mathrm{St}}{\rho}\frac{1}{S_0(t)^3}, \tag{4.27d}$$

$$t^* \approx \frac{\rho}{6k\mathrm{St}}. \tag{4.27e}$$

4.4 Discussion and summary of the solutions

In this section, we have considered the three subregimes that arise from taking the small Stefan number limit to solve the problems found in regime i, after first taking the large Lewis number limit. As we have mentioned, our analysis for this regime is similar to that of McCue et al. [30]. However, we remark that, with their definition of the Stefan number, this analysis corresponds to their large Stefan number limit. After calculating the solutions, which are given in (4.9), (4.19) and (4.27), we notice that at leading order, the solutions in subregimes i(1) and i(3) are linearisations of the solution in subregime i(2). Therefore, to find the leading-order behaviour when we expand in St, it is enough to consider the solution in subregime i(2).

Finally, we need to discuss the validity of the analysis, given that we have taken first the limit $\epsilon \to 0$ and second the limit $\mathrm{St} \to 0$. The physical meaning of the limit $\epsilon \to 0$ is that mass diffusion happens at a much slower timescale than heat diffusion does. The limit $\mathrm{St} \to 0$ means that the timescale of the motion of the interface is much smaller than the thermal diffusive timescale. We expect that the concentration profile to be driven by the motion of the interface, which corresponds to the limit $\epsilon \ll \mathrm{St} \ll 1$, which in terms of timescales means that the solute diffusion timescale is much smaller than the interface motion timescale, which in turn is much smaller than the heat diffusion timescale. Mathematically, this condition ensures that we can first take the small epsilon limit, and second the small Stefan number limit. However, we shall in practice use the more restrictive condition of $\epsilon^{2/3} \ll \mathrm{St}$, which arises from considering that subregime i(3) happens before regime ii. We have that, when $S = \mathcal{O}\left(\epsilon^{1/3}\right)$, the concentration at the interface $c_i = \mathcal{O}\left(\epsilon^{-1}\right)$, and thus we need to consider another regime. Knowing that in subregime i(3), the interface position is $S = \mathcal{O}(\sqrt{\mathrm{St}})$, in order for subregime i(3) to happen before regime ii, we require $\sqrt{\mathrm{St}} \gg \epsilon^{1/3}$. Notice that in [30], the authors consider a fourth timescale, which is exponentially small. However, regime ii happens before this new subregime, as long as $\epsilon \gg \exp\left(-3\sqrt{\frac{2\pi}{\mathrm{St}}}\right)$ (which is satisfied for our problem), as well.

5 Asymptotic solutions in regime ii

We now consider the transition region, regime ii. In this regime, the interface is still far away from the centre, so we need to distinguish three layers: the outer layer D in the solid, the thermal inner layer E near the centre of the cast and the concentration inner layer F around the moving interface.

https://doi.org/10.1017/S095679252000011X Published online by Cambridge University Press

5.1 Layer *D*

We consider first the outer layer in the solid. Taking the scalings $t = t^* + \epsilon^{\frac{2}{3}}\tau$, $S = \epsilon^{\frac{1}{3}}\hat{S}$ and $c_s = \epsilon\hat{c}_s$, we find that

$$\frac{\partial \hat{c}_s}{\partial t} = \epsilon^{\frac{8}{3}}\hat{D}\left(\frac{\partial^2 \hat{c}_s}{\partial r^2} + \frac{2}{r}\frac{\partial \hat{c}_s}{\partial r}\right), \quad \frac{\partial T_s}{\partial t} = \epsilon^{\frac{2}{3}}\kappa\left(\frac{\partial^2 T_s}{\partial r^2} + \frac{2}{r}\frac{\partial T_s}{\partial r}\right), \quad \text{for } 0 < r < 1, \tag{5.1a}$$

$$\frac{\partial \hat{c}_s}{\partial r} = 0 \quad \text{and} \quad T_s = -1, \quad \text{at } r = 1, \tag{5.1b}$$

and with boundary conditions at $r = 0$ given by the matching with layer *E*. Initial conditions are given by the matching with layer *A*. At leading order, we find that the solutions are constant in time, and using the matching conditions, which are detailed in Section 5.4, we conclude that

$$c_s = \epsilon\hat{\alpha}\frac{\hat{c}_0}{3}\frac{k\mathrm{St}}{\rho}\frac{1 - r^3}{(1 - r)r^3} \quad \text{and} \quad T_s = -1. \tag{5.2}$$

5.2 Layer *E*

Now, we consider the inner layer of size $(\epsilon^{\frac{1}{3}})$ around the centre of the sphere. This layer comprises both phases, and it is in this layer where we see thermal diffusion. We use the rescalings $t = t^* + \epsilon^{\frac{2}{3}}\tau$, $r = \epsilon^{\frac{1}{3}}\xi$, $S = \epsilon^{\frac{1}{3}}\hat{S}$ and $c_l = \epsilon\hat{c}_l$, so that we can write down the problem for this layer:

$$\frac{\partial c_s}{\partial \tau} = \epsilon^2\hat{D}\left(\frac{\partial^2 c_s}{\partial \xi^2} + \frac{2}{\xi}\frac{\partial c_s}{\partial \xi}\right), \quad \frac{\partial T_s}{\partial \tau} = \kappa\left(\frac{\partial^2 T_s}{\partial \xi^2} + \frac{2}{\xi}\frac{\partial T_s}{\partial \xi}\right), \quad \text{for } \xi > \hat{S}(\tau), \tag{5.3a}$$

$$\frac{\partial \hat{c}_l}{\partial \tau} = \epsilon\left(\frac{\partial^2 \hat{c}_l}{\partial \xi^2} + \frac{2}{\xi}\frac{\partial \hat{c}_l}{\partial \xi}\right), \quad \frac{\partial T_l}{\partial \tau} = \frac{\partial^2 T_l}{\partial \xi^2} + \frac{2}{\xi}\frac{\partial T_l}{\partial \xi}, \quad \text{for } 0 < \xi < \hat{S}(\tau), \tag{5.3b}$$

$$\frac{\partial \hat{c}_l}{\partial \xi} = 0 \quad \text{and} \quad \frac{\partial T_l}{\partial \xi} = 0, \quad \text{at } \xi = 0. \tag{5.3c}$$

In this layer, we have no interface conditions, as they are imposed through the matching with layer *F* in each phase. The remaining conditions are found by matching the solutions with layer *D*. At $\mathcal{O}(1)$, the problem is

$$\frac{\partial c_{s0}}{\partial \tau} = 0, \quad \frac{\partial T_{s0}}{\partial \tau} = \kappa\left(\frac{\partial^2 T_{s0}}{\partial \xi^2} + \frac{2}{\xi}\frac{\partial T_{s0}}{\partial \xi}\right), \quad \text{for } \xi > \hat{S}(\tau), \tag{5.4a}$$

$$\frac{\partial \hat{c}_{l0}}{\partial \tau} = 0, \quad \frac{\partial T_{l0}}{\partial \tau} = \frac{\partial^2 T_{l0}}{\partial \xi^2} + \frac{2}{\xi}\frac{\partial T_{l0}}{\partial \xi}, \quad \text{for } 0 < \xi < \hat{S}(\tau), \tag{5.4b}$$

$$\frac{\partial \hat{c}_{l0}}{\partial \xi} = 0 \quad \text{and} \quad \frac{\partial T_{l0}}{\partial \xi} = 0, \quad \text{at } \xi = 0. \tag{5.4c}$$

We can immediately determine the concentrations $c_s = \hat{\alpha}c_i(\hat{S}_0^{-1}(\xi))$ and $c_l = \epsilon\hat{c}_0$, where for c_s we have used the matching condition with layer *F* and for c_l we have used the matching condition with layer *C*.

For the temperature fields, we need the extra conditions given by the matching with layers *D* and *F*. The details of the matching are shown in Section 5.4, but they give the leading-order

https://doi.org/10.1017/S095679252000011X Published online by Cambridge University Press

boundary conditions

$$T_{s0} = T_{l0} = -\frac{c_{i0}(\tau)}{\hat{m}_l}, \quad \frac{\rho}{\mathrm{St}}\frac{\mathrm{d}\hat{S}_0}{\mathrm{d}\tau} = k\frac{\partial T_{s0}}{\partial \xi} - \frac{\partial T_{l0}}{\partial \xi}, \quad \text{at } \xi = \hat{S}_0(\tau), \tag{5.5a}$$

$$\frac{\partial T_{l0}}{\partial \xi} = 0, \quad \text{at} \quad \xi = 0, \quad \text{and} \quad T_{s0} \to -1, \quad \text{as} \quad \xi \to +\infty, \tag{5.5b}$$

where $c_{i0}(\tau)$ is the solution of

$$c_{i0}'(\tau) + c_{i0}(\tau)\left(\hat{\alpha}\hat{S}_0'(\tau)^2 + 2\frac{\hat{S}_0'(\tau)}{\hat{S}_0(\tau)} - \frac{\hat{S}_0''(\tau)}{\hat{S}_0'(\tau)}\right) = 0. \tag{5.6}$$

The initial conditions are provided by the matching with regime i.

We cannot obtain exact solutions to this problem, but we can find asymptotic approximations in the limit $\mathrm{St} \to 0$. We introduce the scalings $\tau = \mathrm{St}^{-\frac{1}{3}}\tilde{\tau}$, $\xi = \mathrm{St}^{\frac{1}{3}}\tilde{\xi}$ and $\hat{S}_0 = \mathrm{St}^{\frac{1}{3}}\tilde{S}_0$, which transforms (5.5) to

$$\mathrm{St}\frac{\partial T_{s0}}{\partial \tilde{\tau}} = \kappa\left(\frac{\partial^2 T_{s0}}{\partial \tilde{\xi}^2} + \frac{2}{\tilde{\xi}}\frac{\partial T_{s0}}{\partial \tilde{\xi}}\right), \quad \text{for } \tilde{\xi} > \tilde{S}_0(\tilde{\tau}), \tag{5.7a}$$

$$\mathrm{St}\frac{\partial T_{l0}}{\partial \tilde{\tau}} = \frac{\partial^2 T_{l0}}{\partial \tilde{\xi}^2} + \frac{2}{\tilde{\xi}}\frac{\partial T_{l0}}{\partial \tilde{\xi}}, \quad \text{for } 0 < \tilde{\xi} < \tilde{S}_0(\tilde{\tau}), \tag{5.7b}$$

$$T_{s0} = T_{l0} = -\frac{c_{i0}(\tilde{\tau})}{\hat{m}_l}, \quad \rho\frac{\mathrm{d}\tilde{S}_0}{\mathrm{d}\tilde{\tau}} = k\frac{\partial T_{s0}}{\partial \tilde{\xi}} - \frac{\partial T_{l0}}{\partial \tilde{\xi}}, \quad \text{at } \tilde{\xi} = \tilde{S}_0(\tilde{\tau}), \tag{5.7c}$$

$$\frac{\partial T_{l0}}{\partial \tilde{\xi}} = 0, \quad \text{at } \tilde{\xi} = 0, \quad \text{and} \quad T_{s0} \to -1, \quad \text{as } \tilde{\xi} \to +\infty, \tag{5.7d}$$

$$c_{i0}'(\tilde{\tau}) + c_{i0}(\tilde{\tau})\left(\mathrm{St}\hat{\alpha}\tilde{S}_0'(\tilde{\tau})^2 + 2\frac{\tilde{S}_0'(\tilde{\tau})}{\tilde{S}_0(\tilde{\tau})} - \frac{\tilde{S}_0''(\tilde{\tau})}{\tilde{S}_0'(\tilde{\tau})}\right) = 0. \tag{5.7e}$$

The condition when $\tilde{\xi} \to +\infty$ comes from considering the outer layer (within which we have not rescaled ξ), which gives that at leading order the temperature is constant in time. Matching shows that temperature is homogeneous in space and equal to -1.

We take $\tilde{\xi}$ and $\tilde{S}_0$ as the independent variables, with T_{s0}, T_{l0}, c_{i0} and $\tilde{\tau}$ as the dependent variables, and we expand them in powers of St using the notation $T_{s0} = T_{s0,0} + \mathrm{St}T_{s0,1} + \mathcal{O}\left(\mathrm{St}^2\right)$, $T_{l0} = T_{l0,0} + \mathrm{St}T_{l0,1} + \mathcal{O}\left(\mathrm{St}^2\right)$, $c_{i0} = c_{i0,0} + \mathrm{St}c_{i0,1} + \mathcal{O}\left(\mathrm{St}^2\right)$, $\tilde{\tau} = \tilde{\tau}_{,0} + \mathrm{St}\tilde{\tau}_{,1} + \mathcal{O}\left(\mathrm{St}^2\right)$. Using these expansions in (5.7), we find that at $\mathcal{O}(1)$ the problem is

$$\frac{\partial^2 T_{s0,0}}{\partial \tilde{\xi}^2} + \frac{2}{\tilde{\xi}}\frac{\partial T_{s0,0}}{\partial \tilde{\xi}} = 0, \quad \text{for } \tilde{\xi} > \tilde{S}_0, \qquad \frac{\partial^2 T_{l0,0}}{\partial \tilde{\xi}^2} + \frac{2}{\tilde{\xi}}\frac{\partial T_{l0,0}}{\partial \tilde{\xi}} = 0, \quad \text{for } 0 < \tilde{\xi} < \tilde{S}_0, \tag{5.8a}$$

$$T_{s0,0} = T_{l0,0} = -\frac{c_{i0,0}(\tilde{S}_0)}{\hat{m}_l}, \quad \rho = \frac{\mathrm{d}\tilde{\tau}_{,0}}{\mathrm{d}\tilde{S}_0}\left(k\frac{\partial T_{s0,0}}{\partial \tilde{\xi}} - \frac{\partial T_{l0,0}}{\partial \tilde{\xi}}\right), \quad \text{at } \tilde{\xi} = \tilde{S}_0, \tag{5.8b}$$

https://doi.org/10.1017/S095679252000011X Published online by Cambridge University Press

$$\frac{\partial T_{l0,0}}{\partial \tilde{\xi}} = 0, \quad \text{at} \quad \tilde{\xi} = 0, \quad \text{and} \quad T_{s0,0} \to -1, \quad \text{as} \quad \tilde{\xi} \to +\infty, \tag{5.8c}$$

$$c'_{i0,0}(\tilde{S}_0)\tilde{\tau}'_{,0}(\tilde{S}_0) + c_{i0,0}(\tilde{S}_0)\left(\frac{2}{\tilde{S}_0}\tilde{\tau}'_{,0}(\tilde{S}_0) + \tilde{\tau}''_{,0}(\tilde{S}_0)\right) = 0. \tag{5.8d}$$

We solve (5.8), finding

$$T_{s0,0} = -1 + \left(-\frac{c_{i0,0}(\tilde{S}_0)}{\hat{m}_l} + 1\right)\frac{\tilde{S}_0}{\tilde{\xi}}, \quad T_{l0,0} = -\frac{c_{i0,0}(\tilde{S}_0)}{\hat{m}_l}, \quad c_{i0,0} = \frac{C_2}{\tilde{S}_0^2\tilde{\tau}'_{,0}(\tilde{S}_0)}, \tag{5.9}$$

where C_2 is a constant yet to be determined.

We substitute these expressions into (5.8d), to find

$$\tilde{\tau}_{,0} = -\frac{C_2}{\hat{m}_l}\frac{1}{\tilde{S}_0} - \frac{\rho}{2k}\tilde{S}_0^2 + C_3, \quad c_{i0,0} = \frac{C_2 k\hat{m}_l}{C_2 k - \hat{m}_l\rho\tilde{S}_0^3}. \tag{5.10}$$

where C_3 is a constant. We can determine C_2 by matching concentration at the interface with regime i(3) and, as shown later in Section 5.4, $C_2 = -\frac{\hat{c}_0}{3}$. Substituting this expression back into (5.10) and (5.9), and rescaling using original variables,

$$\tau \approx \frac{\hat{c}_0}{3\hat{m}_l}\frac{1}{\hat{S}_0} - \frac{\rho}{2\mathrm{St}k}\hat{S}_0^2 + \tau^*, \quad c_{i0} \approx \frac{\hat{c}_0 k\mathrm{St}\hat{m}_l}{\hat{c}_0 k\mathrm{St} + 3\hat{m}_l\rho\hat{S}_0^3}, \tag{5.11}$$

where $\tau^* = \mathrm{St}^{-\frac{1}{3}}C_3$ is a time shift (which we do not consider here).

5.3 Layer *F*

We finally study the layer F. This layer is of thickness $(\epsilon^{\frac{4}{3}})$ around the moving boundary, and it is in this layer where we observe both diffusion and advection (the latter due to the moving boundary) of impurities in the liquid phase. The rescaling for this layer is $t = t^* + \epsilon^{\frac{2}{3}}\tau$, $r = \epsilon^{\frac{1}{3}}(\hat{S}(\tau) + \epsilon R)$, $S = \epsilon^{\frac{1}{3}}\hat{S}$ and $c_l = \epsilon^{-1}\hat{c}_l$. For $R > 0$, we have

$$\epsilon\frac{\partial c_s}{\partial \tau} = \hat{S}'(\tau)\frac{\partial c_s}{\partial R} + \epsilon\hat{D}\left(\frac{\partial^2 c_s}{\partial R^2} + \epsilon\frac{2}{\hat{S}(\tau) + \epsilon R}\frac{\partial c_s}{\partial R}\right), \tag{5.12a}$$

$$\epsilon^2\frac{\partial T_s}{\partial \tau} = \epsilon\hat{S}'(\tau)\frac{\partial T_s}{\partial R} + \kappa\left(\frac{\partial^2 T_s}{\partial R^2} + \epsilon\frac{2}{\hat{S}(\tau) + \epsilon R}\frac{\partial T_s}{\partial R}\right), \tag{5.12b}$$

for $R < 0$, we have

$$\epsilon\frac{\partial \hat{c}_l}{\partial \tau} = \hat{S}'(\tau)\frac{\partial \hat{c}_l}{\partial R} + \frac{\partial^2 \hat{c}_l}{\partial R^2} + \epsilon\frac{2}{\hat{S}(\tau) + \epsilon R}\frac{\partial \hat{c}_l}{\partial R}, \tag{5.12c}$$

$$\epsilon^2\frac{\partial T_l}{\partial \tau} = \epsilon\hat{S}'(\tau)\frac{\partial T_l}{\partial R} + \frac{\partial^2 T_l}{\partial R^2} + \epsilon\frac{2}{\hat{S}(\tau) + \epsilon R}\frac{\partial T_l}{\partial R}, \tag{5.12d}$$

https://doi.org/10.1017/S095679252000011X Published online by Cambridge University Press

and at the interface, $R = 0$, we have

$$T_s = T_l, \quad c_s = \hat{\alpha}\hat{c}_l, \quad \hat{c}_l = -\hat{m}_l T_l, \quad \epsilon \frac{\rho}{\mathrm{St}} \frac{\mathrm{d}\hat{S}}{\mathrm{d}\tau} = k \frac{\partial T_s}{\partial R} - \frac{\partial T_l}{\partial R},$$

$$\text{and} \quad (1 - \epsilon\hat{\alpha})\hat{c}_l \frac{\mathrm{d}\hat{S}}{\mathrm{d}\tau} = \epsilon^2 \hat{D} \frac{\partial c_s}{\partial R} - \frac{\partial \hat{c}_l}{\partial R}. \tag{5.12e}$$

Notice that this is almost the same problem as in layer B, therefore we do not detail the solution procedure here. We expand in powers of $\epsilon^{\frac{1}{3}}$, due to the matching with layer E, and find that the solutions are

$$c_s = \hat{\alpha} c_{i0}(\tau) + \epsilon^{\frac{1}{3}} \hat{\alpha} c_{i\frac{1}{3}}(\tau) + \epsilon^{\frac{2}{3}} \hat{\alpha} c_{i\frac{2}{3}}(\tau) + \epsilon \left(\frac{\hat{\alpha} c_{i0}(\tau)}{\hat{S}_0'(\tau)} R + \hat{\alpha} c_{i1}(\tau) \right), \tag{5.13a}$$

$$\begin{aligned} c_l = {} & \epsilon^{-1} c_{i0}(\tau) e^{-\hat{S}_0'(\tau)R} + \epsilon^{-\frac{2}{3}} \left(c_{i\frac{1}{3}}(\tau) - R c_{i0}(\tau) \hat{S}_{\frac{1}{3}}'(\tau) \right) e^{-\hat{S}_0'(\tau)R} \\ & + \epsilon^{-\frac{1}{3}} \left(c_{i\frac{2}{3}}(\tau) - R \left(c_{i\frac{1}{3}}(\tau) \hat{S}_{\frac{1}{3}}'(\tau) + c_{i0}(\tau) \hat{S}_{\frac{2}{3}}'(\tau) \right) + \frac{R^2}{2} c_{i0}(\tau) \hat{S}_{\frac{1}{3}}'(\tau) \right) e^{-\hat{S}_0'(\tau)R} \\ & + \left(\mathcal{A}_1(\tau) + (c_{i1}(\tau) - \mathcal{A}_1(\tau) + R\mathcal{A}_2(\tau, R)) \, e^{-\hat{S}_0'(\tau)R} \right), \end{aligned} \tag{5.13b}$$

$$T_s = -\frac{c_{i0}(\tau)}{\hat{m}_l} - \epsilon^{\frac{1}{3}} \frac{c_{i\frac{1}{3}}(\tau)}{\hat{m}_l} - \epsilon^{\frac{2}{3}} \frac{c_{i\frac{2}{3}}(\tau)}{\hat{m}_l} + \epsilon \left(A_4(\tau) R - \frac{c_{i1}(\tau)}{\hat{m}_l} \right), \tag{5.13c}$$

$$T_l = -\frac{c_{i0}(\tau)}{\hat{m}_l} - \epsilon^{\frac{1}{3}} \frac{c_{i\frac{1}{3}}(\tau)}{\hat{m}_l} - \epsilon^{\frac{2}{3}} \frac{c_{i\frac{2}{3}}(\tau)}{\hat{m}_l} + \epsilon \left(\left(k A_4(\tau) - \frac{\rho}{\mathrm{St}} \hat{S}_0'(\tau) \right) R - \frac{c_{i1}(\tau)}{\hat{m}_l} \right), \tag{5.13d}$$

with

$$\mathcal{A}_1(\tau) = \frac{c_{i0}'(\tau)}{\hat{S}_0'(\tau)^2} + c_{i0}(\tau) \left(\hat{\alpha} + \frac{2}{\hat{S}_0(\tau)\hat{S}_0'(\tau)} - \frac{\hat{S}_0''(\tau)}{\hat{S}_0'(\tau)^3} \right), \tag{5.14a}$$

$$\begin{aligned} \mathcal{A}_2(\tau, R) = {} & -\frac{c_{i0}'(\tau)}{\hat{S}_0'(\tau)} - c_{i\frac{2}{3}} \hat{S}_1'(\tau) + \frac{1}{2} c_{i\frac{1}{3}}(\tau) \left(R \hat{S}_{\frac{1}{3}}'(\tau)^2 - 2\hat{S}_2' 3(\tau) \right) \\ & + c_{i0}(\tau) \left(-\frac{2}{\hat{S}_0(\tau)} - \frac{R^2}{6} \hat{S}_{\frac{1}{3}}'(\tau)^3 + R \hat{S}_{\frac{1}{3}}' \hat{S}_{\frac{2}{3}}' - \hat{S}_1'(\tau) + \left(1 + \frac{R}{2} \hat{S}_0'(\tau) \right) \frac{\hat{S}_0''(\tau)}{\hat{S}_0'(\tau)^2} \right), \end{aligned} \tag{5.14b}$$

where $c_{i0}(\tau)$ and $A_4(\tau)$ are determined from matching. The values of $c_{i\frac{1}{3}}$, $c_{i\frac{2}{3}}$ and c_{i1} require matching of higher order solutions not presented here.

5.4 Matching of the solutions

In this section, we detail the matching between the solutions of the different layers that we have used in the previous sections to fully determine the problem.

We start matching layer D with layer A to obtain the initial conditions that determine the leading-order solutions in layer D. The matching for c_s is trivial, as the solution is independent of time in both layers. For T_s, we take one term in the inner solution and one term in the

https://doi.org/10.1017/S095679252000011X Published online by Cambridge University Press

outer solution, finding $-1 = (1\text{ti})(1\text{to}) = (1\text{to})(1\text{ti}) = \lim_{\tau\to-\infty} T_{s0}$, so we can fully determine the leading-order solutions in layer D. Similarly, we can match c_l and T_l between layers C and E.

We now have to match the space layer D with layer E, which provides the boundary condition needed for T_s (it is not necessary to match for c_s, as at leading order the condition is not required). Then, taking one term in both the inner and outer solutions, we find $-1 = (1\text{ti})(1\text{to}) = (1\text{to})(1\text{ti}) = \lim_{\xi\to+\infty} T_{s0}$.

The next layers we have to match are layers E and F. We start by matching the temperature fields, both in the solid and the liquid, taking two terms in the inner and the outer solutions. For the solid, we match

$$(2\text{ti})(2\text{to}) = T_{s0}(\tau, \hat{S}_0(\tau)) + \epsilon^{\frac{1}{3}}\,(\cdots) + \epsilon^{\frac{2}{3}}\,(\cdots) + \epsilon\left((\cdots) + \left(R + \hat{S}_1(\tau)\right)\left.\frac{\partial T_{s0}}{\partial \xi}\right|_{\xi=\hat{S}_0}\right), \tag{5.15a}$$

$$(2\text{to})(2\text{ti}) = -\frac{c_{i0}(\tau)}{\hat{m}_l} - \epsilon^{\frac{1}{3}}\frac{c_{i\frac{1}{3}}(\tau)}{\hat{m}_l} - \epsilon^{\frac{2}{3}}\frac{c_{i\frac{2}{3}}(\tau)}{\hat{m}_l} + \epsilon\left(RA_4(\tau) - \frac{c_{i1}(\tau)}{\hat{m}_l}\right). \tag{5.15b}$$

The $(\cdots)$ here represents terms that are known, as shown in (5.13), but not necessary for the matching, given the purpose of our analysis. Therefore, to simplify the notation, we do not reproduce these terms here. We conclude

$$T_{s0}(\tau, \hat{S}_0(\tau)) = -\frac{c_{i0}(\tau)}{\hat{m}_l}, \quad A_4(\tau) = \left.\frac{\partial T_{s0}}{\partial \xi}\right|_{\xi=\hat{S}_0}. \tag{5.16a}$$

In the liquid, we match

$$(2\text{ti})(2\text{to}) = T_{l0}(\tau, \hat{S}_0(\tau)) + \epsilon^{\frac{1}{3}}\,(\cdots) + \epsilon^{\frac{2}{3}}\,(\cdots) + \epsilon\left((\cdots) + \left(R + \hat{S}_1(\tau)\right)\left.\frac{\partial T_{l0}}{\partial \xi}\right|_{\xi=\hat{S}_0}\right), \tag{5.17a}$$

$$(2\text{to})(2\text{ti}) = -\frac{c_{i0}(\tau)}{\hat{m}_l} - \epsilon^{\frac{1}{3}}\frac{c_{i\frac{1}{3}}(\tau)}{\hat{m}_l} - \epsilon^{\frac{2}{3}}\frac{c_{i\frac{2}{3}}(\tau)}{\hat{m}_l} + \epsilon\left(\left(kA_4(\tau) - \frac{\rho}{\mathrm{St}}\frac{\mathrm{d}\hat{S}_0}{\mathrm{d}\tau}\right)R - \frac{c_{i1}(\tau)}{\hat{m}_l}\right), \tag{5.17b}$$

which gives

$$T_{l0}(\tau, \hat{S}_0(\tau)) = -\frac{c_{i0}(\tau)}{\hat{m}_l}, \quad kA_4(\tau) - \frac{\rho}{\mathrm{St}}\frac{\mathrm{d}\hat{S}_0}{\mathrm{d}\tau} = \left.\frac{\partial T_{l0}}{\partial \xi}\right|_{\xi=\hat{S}_0}. \tag{5.18}$$

We have the boundary conditions for both T_{s0} and T_{l0} in layer E, as well as the Stefan condition

$$\frac{\rho}{\mathrm{St}}\frac{\mathrm{d}\hat{S}_0}{\mathrm{d}\tau} = k\left.\frac{\partial T_{s0}}{\partial \xi}\right|_{\xi=\hat{S}_0} - \left.\frac{\partial T_{l0}}{\partial \xi}\right|_{\xi=\hat{S}_0}, \tag{5.19}$$

so we have fully determined the problem (5.5).

Matching c_s between layers E and F, we find $c_{s0}(\hat{S}_0(\tau)) = (1\text{ti})(1\text{to}) = (1\text{to})(1\text{ti}) = \hat{\alpha}c_i(\tau)$. In order to match c_l between layers E and F, we proceed in the same way as we did to match between layers B and C, finding $\mathcal{A}_1(\tau) = (1\text{ti})(1\text{to}) = (1\text{to})(1\text{ti}) = 0$, which gives

$$\frac{c'_{i0}(\tau)}{\hat{S}'_0(\tau)^2} + c_{i0}(\tau)\left(\hat{\alpha} + \frac{2}{\hat{S}_0(\tau)\hat{S}'_0(\tau)} - \frac{\hat{S}''_0(\tau)}{\hat{S}'_0(\tau)^3}\right) = 0. \tag{5.20}$$

https://doi.org/10.1017/S095679252000011X Published online by Cambridge University Press

Finally, we need to match c_i between regimes i and ii, where regime i acts as the outer layer and ii as the inner layer. This matching determines $\hat{S}_0(\tau)$ up to a time shift, which requires higher order matching and is not studied here. For simplicity, we take c_i as a function of $\hat{S}_0$. Using $\hat{S}_0 = \mathrm{St}^{\frac{1}{3}}\tilde{S}_0$, we rescale (5.9) like

$$c_{i0}(\hat{S}_0) = \frac{C_2 \mathrm{St} k \hat{m}_l}{C_2 \mathrm{St} k - \hat{m}_l \rho \hat{S}_0^3}. \tag{5.21}$$

Now, using that $S_0 = \epsilon^{\frac{1}{3}}\hat{S}_0$, we can take the inner solution up to $\mathcal{O}\left(\epsilon^{-1}\right)$ and the outer solution up to $\mathcal{O}(1)$, finding $\frac{\hat{c}_0}{3}\frac{k\mathrm{St}}{\rho}\frac{1}{\hat{S}_0^3}\epsilon^{-1} = (1\mathrm{ti})(1\mathrm{to}) = (1\mathrm{to})(1\mathrm{ti}) = -C_2\frac{k\mathrm{St}}{\rho}\frac{1}{\hat{S}_0^3}\epsilon^{-1}$, hence $C_2 = -\frac{\hat{c}_0}{3}$.

This concludes the analysis of regime ii. In this regime, we have observed how the solidification process is driven by a build-up of the interfacial concentration due to rejection from the solid phase. This build-up causes a decrease in the interfacial temperature due to constitutional supercooling and, therefore, a decrease in the thermal gradients at the interface that slows down the motion of the solidification front. At the end of this regime, when $\tau \to +\infty$, we find that the position of the interface at leading order goes to zero. That means that the liquid part of layer E vanishes, and therefore, we need to consider another regime in which the impurity diffusion inner layer now notices the symmetry boundary condition at $r = 0$.

6 Asymptotic solutions in regime iii

We finally consider regime iii. In this regime, the interface is at a distance $(\epsilon^{2/3})$ from the origin and we need to distinguish two different layers, namely the outer layer in the solid, G, and the inner layer, H, that comprises both phases.

6.1 Layer G

We first consider the outer layer in the solid. Taking the scalings $t = t^* + \epsilon^{\frac{1}{3}}\theta$, $S = \epsilon^{\frac{2}{3}}\hat{S}$ and $c_s = \epsilon\hat{c}_s$, we find

$$\frac{\partial \hat{c}_s}{\partial \theta} = \epsilon^{\frac{7}{3}}\hat{D}\left(\frac{\partial^2 \hat{c}_s}{\partial r^2} + \frac{2}{r}\frac{\partial \hat{c}_s}{\partial r}\right), \quad \frac{\partial T_s}{\partial \theta} = \epsilon^{\frac{1}{3}}\kappa\left(\frac{\partial^2 T_s}{\partial r^2} + \frac{2}{r}\frac{\partial T_s}{\partial r}\right), \quad \text{for } 0 < r < 1, \tag{6.1a}$$

$$\frac{\partial \hat{c}_s}{\partial r} = 0 \quad \text{and} \quad T_s = -1, \quad \text{at } r = 1, \tag{6.1b}$$

and with the remaining conditions given by the matching with layers D and H. At leading order, the solutions are constant in time, and from the matching given in Section 6.3, we conclude $c_s = \epsilon\hat{\alpha}c_i\left(S_0^{-1}(r)\right)$, $T_s = -1$.

6.2 Layer H

Finally, we consider the inner layer H of thickness $(\epsilon^{\frac{2}{3}})$ around the origin. In this layer, the scalings are $t = t^* + \epsilon^{\frac{1}{3}}\theta$, $r = \epsilon^{\frac{2}{3}}R$, $S = \epsilon^{\frac{2}{3}}\hat{S}$ and $c_l = \epsilon^{-1}\hat{c}_l$. We find

$$\frac{\partial c_s}{\partial \theta} = \epsilon\hat{D}\left(\frac{\partial^2 c_s}{\partial R^2} + \frac{2}{R}\frac{\partial c_s}{\partial R}\right), \quad \epsilon\frac{\partial T_s}{\partial \theta} = \kappa\left(\frac{\partial^2 T_s}{\partial R^2} + \frac{2}{R}\frac{\partial T_s}{\partial R}\right), \quad \text{for } R > \hat{S}(\theta), \tag{6.2a}$$

https://doi.org/10.1017/S095679252000011X Published online by Cambridge University Press

$$\frac{\partial \hat{c}_l}{\partial \theta} = \frac{\partial^2 \hat{c}_l}{\partial R^2} + \frac{2}{R}\frac{\partial \hat{c}_l}{\partial R}, \quad \epsilon \frac{\partial T_l}{\partial \theta} = \frac{\partial^2 T_l}{\partial R^2} + \frac{2}{R}\frac{\partial T_l}{\partial R}, \quad \text{for } R < \hat{S}(\theta), \tag{6.2b}$$

$$T_s = T_l, \;\; c_s = \hat{\alpha}\hat{c}_l, \;\; \hat{c}_l = -\hat{m}_l T_l, \;\; \epsilon \frac{\rho}{\mathrm{St}} \frac{\mathrm{d}\hat{S}}{\mathrm{d}\theta} = k\frac{\partial T_s}{\partial R} - \frac{\partial T_l}{\partial R},$$

$$\text{and} \quad \left(1 - \epsilon\hat{\alpha}\right)\hat{c}_l \frac{\mathrm{d}\hat{S}}{\mathrm{d}\theta} = \epsilon^2 \hat{D}\frac{\partial c_s}{\partial R} - \frac{\partial \hat{c}_l}{\partial R}, \;\; \text{at } R = \hat{S}(\theta), \tag{6.2c}$$

$$\frac{\partial \hat{c}_l}{\partial R} = 0 \quad \text{and} \quad \frac{\partial T_l}{\partial R} = 0, \quad \text{at } R = 0. \tag{6.2d}$$

The remaining conditions come from matching with other layers and are detailed in Section 6.3.

At $\mathcal{O}(1)$, the problem reads

$$\frac{\partial c_{s0}}{\partial \theta} = 0, \quad \frac{\partial^2 T_{s0}}{\partial R^2} + \frac{2}{R}\frac{\partial T_{s0}}{\partial R} = 0, \quad \text{for } R > \hat{S}_0(\theta), \tag{6.3a}$$

$$\frac{\partial \hat{c}_{l0}}{\partial \theta} = \frac{\partial^2 \hat{c}_{l0}}{\partial R^2} + \frac{2}{R}\frac{\partial \hat{c}_{l0}}{\partial R}, \quad \frac{\partial^2 T_{l0}}{\partial R^2} + \frac{2}{R}\frac{\partial T_{l0}}{\partial R} = 0, \quad \text{for } R < \hat{S}_0(\theta), \tag{6.3b}$$

$$T_{s0} = T_{l0}, \;\; c_{s0} = \hat{\alpha}\hat{c}_{l0}, \;\; \hat{c}_{l0} = -\hat{m}_l T_{l0}, \;\; k\frac{\partial T_{s0}}{\partial R} = \frac{\partial T_{l0}}{\partial R},$$

$$\text{and} \quad \hat{c}_{l0}\frac{\mathrm{d}\hat{S}_0}{\mathrm{d}\theta} + \frac{\partial \hat{c}_{l0}}{\partial R} = 0, \;\; \text{at } R = \hat{S}_0(\theta), \tag{6.3c}$$

$$\frac{\partial \hat{c}_{l0}}{\partial R} = 0 \quad \text{and} \quad \frac{\partial T_{l0}}{\partial R} = 0, \quad \text{at } R = 0. \tag{6.3d}$$

Matching with the T_s in layer G derived later in Section 6.3 gives $T_s = T_l = -1$. From here, we conclude that $\hat{c}_{l0} = \hat{m}_l$ at the interface. We also determine that $c_s = \hat{\alpha}\hat{m}_l$. To determine $\hat{c}_{l0}$ and $\hat{S}_0$, it will be useful to introduce the scalings $\hat{c}_{l0} = \hat{m}_l c$, $\hat{S}_0 = \left(\frac{\hat{c}_0}{3\hat{m}_l}\right)^{\frac{1}{3}} S$, $R = \left(\frac{\hat{c}_0}{3\hat{m}_l}\right)^{\frac{1}{3}} r$, $\theta = \left(\frac{\hat{c}_0}{3\hat{m}_l}\right)^{\frac{2}{3}} t$, which results in the parameter-free problem

$$\frac{\partial c}{\partial t} = \frac{\partial^2 c}{\partial r^2} + \frac{2}{r}\frac{\partial c}{\partial r}, \quad \text{in} \quad 0 < r < S(t), \tag{6.4a}$$

$$\frac{\partial c}{\partial r} = 0, \quad \text{at } r = 0, \quad c = 1 \;\text{ and }\; c\frac{\mathrm{d}S}{\mathrm{d}t} + \frac{\partial c}{\partial r} = 0, \quad \text{at } r = S(t), \tag{6.4b}$$

$$c \sim \exp\left(-\frac{\mathrm{d}S}{\mathrm{d}t}\left(r - S(t)\right)\right) \;\text{ and }\; S \sim \frac{1}{t}, \quad \text{when} \quad t \to 0, \tag{6.4c}$$

which is a one-phase Stefan problem describing the impurity diffusion in a shrinking core.

We are unable to determine analytical solutions to this problem. However, as we have eliminated all parameters of the problem, we can calculate the solution numerically. We use a finite volume scheme similar to the one we shall describe in the Appendix, but in this case, it is simpler as we only need to solve the problem for the concentration and the position of the interface. Because of the singularity in the initial condition as $t \to 0$, we have to impose the initial conditions of the numerical scheme at some initial time $t = t_0$ close to zero. As the problem (6.4) with an initial condition at $t = t_0$, with t_0 arbitrarily small, is a classical one-phase Stefan problem with sufficiently smooth data, from Theorem III.2 in [11], we know that the solution on $t \in [t_0, \infty)$ is unique. The different numerical simulations for different values of t_0 seem to converge as $t_0 \to 0$, even though we do not have an analytical proof that in this limit the solution to the problem is unique. Notice as well that the problem is a supercooled Stefan problem, and therefore it could

https://doi.org/10.1017/S095679252000011X Published online by Cambridge University Press

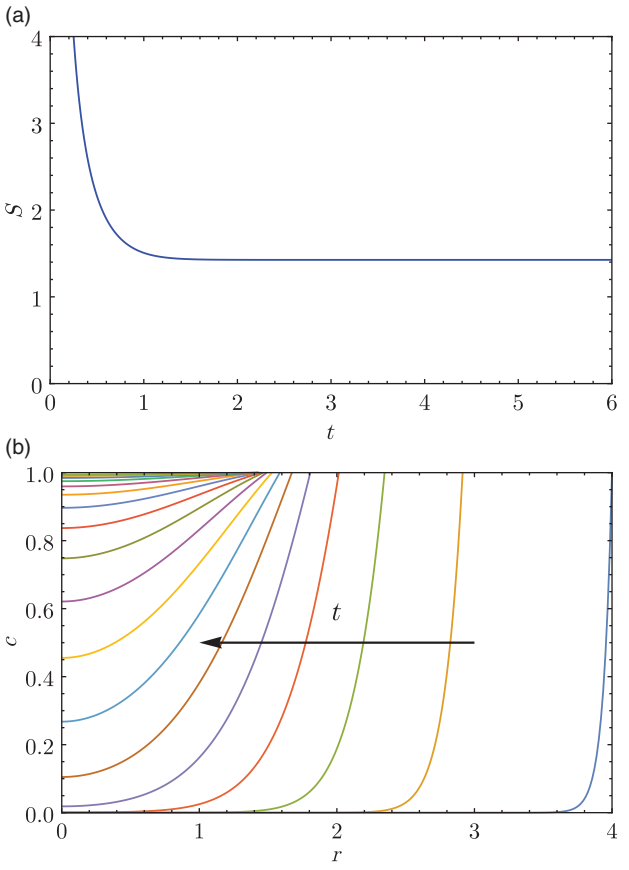

FIGURE 4. Plots of the interface position S over time (a) and concentration profiles c over space for various values of time (b) arising from (6.4). Numerical solutions were obtained using a fixed boundary method and a finite volume scheme.

go unstable. These problems have been studied in the literature [12, 13, 14, 17], but it remains an open question whether this particular problem is stable. The numerical simulations, however, do not show instability. The plots for the position of the interface and the concentration profiles are shown in Figure 4.

Even though we cannot find analytical solutions to the problem (6.4), we can calculate the steady state. One can check that the total amount of impurities in problem (6.4) is conserved. Then, since we know that the steady-state concentration profile is homogeneous in space, we have that the total concentration at the steady state is $c_{\text{tot}} = \frac{4}{3}\pi S_{\text{end}}^3 c_{\text{end}}$, where S_{end} and c_{end} are the interface position and the concentration at the steady state, respectively. Because the total concentration is conserved, c_{tot} must be equal to the initial amount, which is given by

$$\begin{aligned} c_{\text{tot}} &= \lim_{t\to 0} 4\pi \int_0^{S(t)} r^2 \exp\left(-\frac{\mathrm{d}S}{\mathrm{d}t}(r - S(t))\right) \mathrm{d}r \\ &= \lim_{t\to 0} 4\pi \left(1 - 2t^3 + 2t^6\left(1 - e^{-\frac{1}{t^3}}\right)\right) = 4\pi. \end{aligned} \tag{6.5}$$

https://doi.org/10.1017/S095679252000011X Published online by Cambridge University Press

We know that the steady-state concentration is $c_{\text{end}} = 1$, as given by the boundary condition (6.4c), hence we conclude $S_{\text{end}} = \sqrt[3]{3} \approx 1.4423$, which agrees with the numerical result shown in Figure 4(a).

6.3 Matching of the solutions

In this section, we match the solutions of the different layers. We start by matching the temperature and concentration in layer G with the solutions in layer D, $\lim_{\theta\to 0} T_{s0} = (1\text{ti})(1\text{to}) = (1\text{to})(1\text{ti}) = -1$. For $\hat{c}_{s0}$, because the solutions in both layers do not depend on time, the matching is trivial.

The next condition we need to derive is the matching of T_s between layers G and H. Taking one term both in the inner and outer solutions, we find $-1 = (1\text{ti})(1\text{to}) = (1\text{to})(1\text{ti}) = \lim_{R\to+\infty} T_{s0}$, which is used to determine T_{s0}.

Finally, we need to determine the initial conditions used in (6.4). We start with $\hat{c}_{l0}$ which we have to match with the solution found in layer F. Taking the solutions up to $\mathcal{O}\left(\epsilon^{-1}\right)$, we determine the matching condition

$$\lim_{\theta\to 0} \epsilon^{-1}\hat{c}_{l0} = (1\text{ti})(1\text{to}) = (1\text{to})(1\text{ti}) = \lim_{\tau\to+\infty} \epsilon^{-1} c_i(\tau) \exp\left(\frac{\mathrm{d}\hat{S}_0}{\mathrm{d}\tau}\left(R - \hat{S}_0(\tau)\right)\right), \tag{6.6}$$

and we know from the solution in regime ii that $c_i \to \hat{m}_l$ and $\hat{S}_0 \to \frac{\hat{c}_0}{3\hat{m}_l \mathrm{St}}\frac{1}{\tau}$ as $\tau \to +\infty$.

The last condition is the one for $\hat{S}_0(\theta)$. We match the solution in regime iii with the solution in regime ii. Taking the solutions at leading order in each regime (so $\mathcal{O}\left(\epsilon^{1/3}\right)$ in regime ii and $\mathcal{O}\left(\epsilon^{2/3}\right)$ in regime iii), we find

$$\lim_{\theta\to 0} \epsilon^{\frac{2}{3}} S_0 = (1\text{ti})(1\text{to}) = (1\text{to})(1\text{ti}) = \epsilon^{\frac{2}{3}} \frac{\hat{c}_0}{3\hat{m}_l}\frac{1}{\theta}. \tag{6.7}$$

We have now finished the analysis of regime iii and notice that the solutions given here hold up to $\theta \to +\infty$, therefore this is the last regime to consider. With the solutions found in each regime, we can now describe the behaviour of the system (2.2) at leading order for $t \in [0, +\infty)$.

7 Summary of the asymptotic solutions and results

After performing the asymptotic analysis of the extended Stefan problem in the spherically symmetric three-dimensional geometry, we have distinguished three different time regimes with significantly different behaviours of the solution. Similar to what was observed in the finite planar geometry configuration [4], the concentration of impurities in the solid remains constant over time, while the concentration at each point is only determined by the time when it solidified. In this section, we provide the leading-order solutions in each layer. The solutions are written in terms of the original dimensionless parameters (i.e. before rescaling). Recall that we defined the small parameter $\epsilon = \mathrm{Le}^{-1}$.

7.1 Leading-order behaviour of solutions

Regime i corresponds to the beginning of the process and has three different layers: two outer layers, one in the solid phase and one in the liquid phase, and an inner layer around the interface.

https://doi.org/10.1017/S095679252000011X Published online by Cambridge University Press

Recall that, in order to determine the solutions for this layer, we required a further expansion in the small Stefan number, as discussed in Section 4. In the outer layer in the solid ($r > S(t)$, layer A), we have

$$c_s \approx \alpha \frac{c_0}{3} \frac{k\mathrm{St}}{\rho} \mathrm{Le} \frac{1-r^3}{(1-r)r^3}, \tag{7.1a}$$

$$T_s \approx \frac{1}{1-S(t)} \left(\frac{S(t)}{r} - 1 \right), \tag{7.1b}$$

in the transition layer ($r = S(t)$, layer B), we have

$$c_s \approx \alpha c_i(t), \tag{7.1c}$$

$$T_s \approx -\frac{r-S(t)}{(1-S(t))S(t)} - \frac{c_i(t)}{m_l}, \tag{7.1d}$$

$$c_l \approx c_i(t) \exp\left(-\frac{\mathrm{d}S}{\mathrm{d}t} \mathrm{Le}\,(r-S(t)) \right), \tag{7.1e}$$

$$T_l \approx -\frac{c_i(t)}{m_l}, \tag{7.1f}$$

and in the outer layer in the liquid ($r < S(t)$, layer C), we have

$$c_l \approx c_0, \tag{7.1g}$$

$$T_l \approx -\frac{c_i(t)}{m_l} + \frac{2T_0 S(t)}{\pi r} \sum_{n=1}^{\infty} \frac{(-1)^{n+1}}{n} \exp\left(-n^2\pi^2 \int_0^t \frac{\mathrm{d}s}{S(s)^2} \right) \sin\left(\frac{n\pi r}{S(t)} \right), \tag{7.1h}$$

where

$$t \approx \frac{\rho}{k\mathrm{St}} \left(\frac{1}{2}(1-S(t))^2 - \frac{1}{3}(1-S(t))^3 \right) + \frac{1}{6\kappa}(1-S(t))^2 \quad \text{and} \tag{7.1i}$$

$$c_i(t) \approx \frac{c_0}{3} \frac{k\mathrm{St}}{\rho} \mathrm{Le} \frac{1-S(t)^3}{(1-S(t))S(t)^3}. \tag{7.1j}$$

In this regime, the system is driven by the thermal problem since the supercooling is small, and therefore we observe similar behaviour to that described in [30]. The impurity build-up happens only in a small layer around the solidification front. However, in this geometry, because the volume of liquid shrinks as the cube of the position of the interface (as opposed to the linear relation we observed in the finite planar problem), the rejection of impurities is stronger and we observe that the concentration of impurities at the interface is no longer constant but grows in time. This is the reason why the next regime to consider is driven by supercooling while the solidification front is still far away from the centre of the sphere.

Then, in this new regime, the front is still at a distance $\mathcal{O}\left(\epsilon^{1/3}\right)$ from the centre, but the impurity build-up causes a significant change in the melting temperature that affects the dynamics of the solidification front. This corresponds to a time of $\mathcal{O}\left(\epsilon^{2/3}\right)$ around the critical time $t = t^*$. We distinguish three layers: an outer layer in the solid, an intermediate layer $\mathcal{O}\left(\epsilon^{1/3}\right)$ around the centre of the sphere and an inner layer $\mathcal{O}(\epsilon)$ around the solidification front. To obtain analytical solutions, we need to also take the small Stefan number limit. In the outer layer D ($r > 0$), we

https://doi.org/10.1017/S095679252000011X Published online by Cambridge University Press

have

$$c_s \approx \alpha \frac{c_0}{3} \frac{k\mathrm{St}}{\rho} \mathrm{Le} \frac{1-r^3}{(1-r)r^3}, \tag{7.2a}$$

$$T_s \approx -1, \tag{7.2b}$$

in the intermediate layer E ($r > 0$), we have

$$c_s \approx \alpha m_l \left(1 + \frac{3m_l}{c_0} \frac{\rho}{k\mathrm{St}} \frac{r^3}{\mathrm{Le}}\right)^{-1}, \tag{7.2c}$$

$$T_s \approx -1 + \left(-\frac{c_i(t)}{m_l} + 1\right) \frac{S(t)}{r}, \tag{7.2d}$$

$$c_l \approx c_0, \tag{7.2e}$$

$$T_l \approx -\frac{c_i(t)}{m_l}, \tag{7.2f}$$

and in the inner layer F around $r = S(t)$, the solutions are

$$c_s \approx \alpha c_i(t), \tag{7.2g}$$

$$T_s \approx -\frac{c_i(t)}{m_l}, \tag{7.2h}$$

$$c_l \approx c_i(t) \exp\left(-\frac{\mathrm{d}S}{\mathrm{d}t} \mathrm{Le}\,(r - S(t))\right), \tag{7.2i}$$

$$T_l \approx -\frac{c_i(t)}{m_l}, \tag{7.2j}$$

where

$$t \approx \frac{c_0}{3m_l} \mathrm{Le} \frac{1}{S(t)} + \frac{\rho}{2k\mathrm{St}} S(t)^2 + t^* + \epsilon^{\frac{2}{3}} \tau^*, \tag{7.2k}$$

$$c_i \approx m_l \left(1 + \frac{3m_l}{c_0} \frac{\rho}{k\mathrm{St}} \frac{S(t)^3}{\mathrm{Le}}\right)^{-1}, \tag{7.2l}$$

$$t^* \approx \frac{\rho}{6k\mathrm{St}} + \frac{1}{6\kappa}. \tag{7.2m}$$

We observe that the dynamics in this regime are driven by the build-up of impurities at the interface, which causes enough supercooling to decrease the temperature in the whole domain down to the temperature of the boundary. This change in the interface temperature results in a decrease in the thermal gradients, and thus the interface slows down. Because the liquid region is still reasonably large, the impurities can diffuse away from the interface, so we still observe an exponential profile in the impurity concentration.

Finally, we consider regime iii, at a late time $\mathcal{O}\left(\epsilon^{1/3}\right)$ after the critical time $t = t^*$, where the interface is within a distance $\mathcal{O}\left(\epsilon^{2/3}\right)$ of the centre of the sphere. We distinguish two layers: an outer layer in the solid and an inner layer of $\mathcal{O}\left(\epsilon^{2/3}\right)$ around the centre. In the outer layer ($r > 0$,

https://doi.org/10.1017/S095679252000011X Published online by Cambridge University Press

layer G), the solutions are

$$c_s \approx \alpha m_l \left(1 + \frac{3m_l}{c_0}\frac{\rho}{k\mathrm{St}}\frac{r^3}{\mathrm{Le}}\right)^{-1}, \tag{7.3a}$$

$$T_s \approx -1, \tag{7.3b}$$

while in the inner layer around $r = 0$, we have

$$c_s \approx \alpha m_l, \tag{7.3c}$$

$$T_s \approx -1, \tag{7.3d}$$

$$T_l \approx -1, \tag{7.3e}$$

while c_l and S have to be determined numerically. In this layer, the temperature in both phases is identical to the boundary temperature, therefore the thermal problem is in steady state. This means that the concentration at the interface remains constant. The concentration in the liquid and the position of the interface evolve following a classical one-phase Stefan problem, which ensures that total mass is conserved. We plot the position of the interface and the concentration of impurities on the liquid side of the interface in Figure 5 for various parameter values, finding that an increase in St results in faster motion of the interface, whereas an increase in Le results in an increase in the impurity concentration.

7.2 Comparison with numerical simulations

We compare the asymptotic solutions to the results of numerical simulations, where the numerical scheme is discussed in the Appendix. When performing our simulations, we set $\mathrm{St} = 0.1$, $\mathrm{Le} = 1000$, $\rho = 1$, $c_p = 1$, $k = 0.36$, $m_l = 1000$, $c_0 = 0.01$ and $T_0 = 0$, which are parameter values close to metallurgical grade silicon [4]. The reason for taking $\mathrm{Le} = 1000$ and $\mathrm{St} = 0.1$ is to make sure that the condition $\epsilon^{\frac{2}{3}} \ll \mathrm{St} \ll 1$ is satisfied, and thus the asymptotic solutions are valid. We take $N_s = 2 \times 10^3$ grid points in the solid phase, $N_l = 2 \times 10^4$ grid points in the liquid phase and an initial time step of $\Delta t = 10^{-3}$. At each step, we use relaxation iterations to solve the nonlinear system, and we take a relaxation parameter $\omega = 0.1$ and a tolerance of $\delta = 0.01$. To help convergence, if one time step takes more than 100 iterations before converging, and the time step is larger than 10^{-5}, we halve the time step. This algorithm is capable of solving the full problem with a total mass variation smaller than 0.1%.

The comparison between our asymptotic solutions and numerical simulations is shown in Figure 6. We find quite good qualitative agreement, and thus we believe that the asymptotic solutions describe the dynamics of the solidification process for the entire time domain. In the plots, we observe a slight discrepancy between both results in regime ii, which is more noticeable in c_i due to the scale of the solution there relative to the accuracy of the lowest order matched asymptotic solution. The agreement would be improved by calculating higher order terms in the matched asymptotic expansion for the solution in that regime, given that for the solution plotted here we only took the leading-order terms in both St and ϵ expansion, but the result is in qualitative agreement with what one would expect. Figure 6(a) shows the position of the interface as a function of time, and we can clearly observe the behaviour for $t < t^*$, which is similar to the pure material problem [30, 37]. Near the critical time, we observe a rapid transition that slows

https://doi.org/10.1017/S095679252000011X Published online by Cambridge University Press

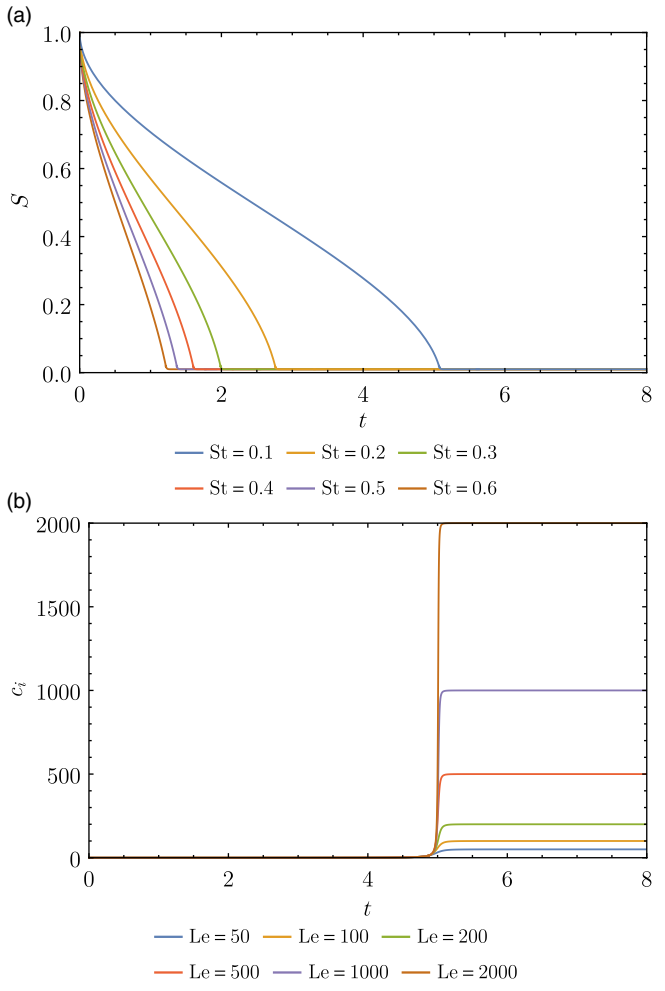

FIGURE 5. Asymptotic solutions for the interface position S as a function of Stefan number St (a) and the concentration of impurities on the liquid side of the interface c_i as a function of Lewis number Le (b).

down the interface, and at late times ($t > t^*$), we see a decay to the steady state at a very small length scale. Figure 6(b) shows the concentration of impurities at the interface as a function of time. At the beginning of the process, we notice that concentration of impurities increases, but remaining of $\mathcal{O}(1)$, while around the critical time there is a very quick build-up until they reach the maximum concentration $c_l = m_l$. Finally, at late time, the concentration remains equal to this maximum value.

7.3 Comparison with experiments

One possible application of our results is to the solidification of metallurgical grade silicon, as explained in previous work [2, 4]. Amongst the various casting techniques used in the silicon industry, we focus here on the water granulation process, in which liquid silicon is solidified into small spherical particles by quenching the molten silicon in a pool of water [31, 32]. Such a process can be described by the model (2.2).

https://doi.org/10.1017/S095679252000011X Published online by Cambridge University Press

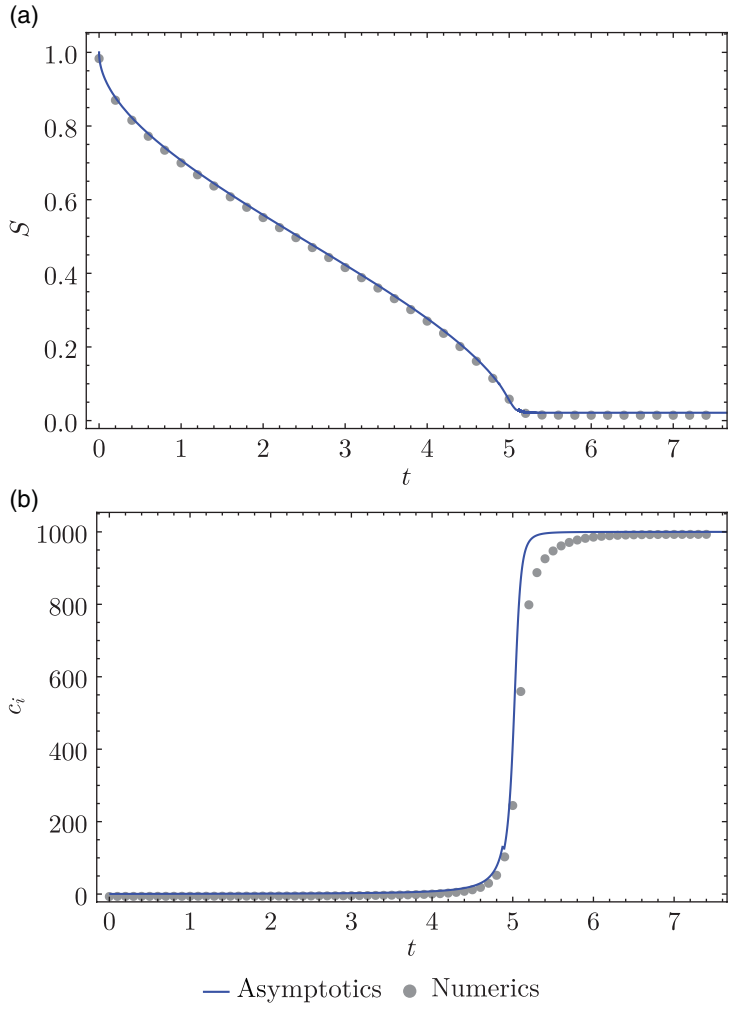

FIGURE 6. Comparison of the asymptotic and numerical solutions for the interface position S (a) and concentration of impurities on the liquid side of the interface c_i (b). The slight discontinuity near $t = 5$ occurs where the solutions are matched across regimes, and including higher order in the matched asymptotic expansions terms would improve the agreement.

The experimental data presented here, which were provided by Elkem, are for two different particles (with diameters 7.5 and 6.0 mm, respectively) of 97% pure silicon cast using water granulation. To measure the distribution of impurities, each particle was polished down to the central cross section, and a scanning electron microscope (SEM) was then used to take a picture of a 1.7-mm-wide band around one of the diameters of the particle. The measurements of the impurity fraction along the diameter were then measured by averaging the values over the direction perpendicular to the diameter at each point. The SEM image of the samples is shown in Figure 7.

The concentration profile in the particle can be described using the expression of c_s in layer E, see (7.3a), as it captures the leading-order behaviour for the whole problem. Given that the

https://doi.org/10.1017/S095679252000011X Published online by Cambridge University Press

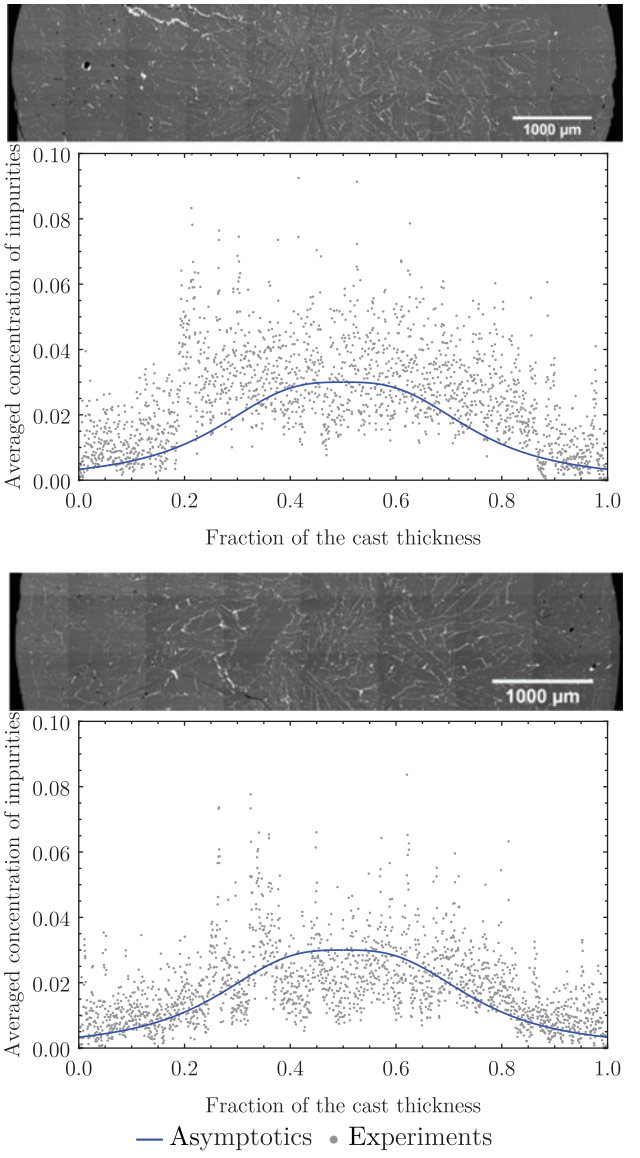

FIGURE 7. Comparison of asymptotic solutions and experimental data for the concentration of impurities (as a volume fraction) in a silicon granule for two distinct samples. Both experimental data and images of the samples have been provided by Elkem. The analytical solution corresponds to (7.4) with parameter values $a = 0.03$ and $b = 8$. The same parameters are used in both samples as they come from the same cast. Notice that, because the data are for the impurities volume fraction and the fraction of the cast thickness, which are dimensionless quantities, we use the dimensionless model directly without the need for rescaling.

experimental data are along the diameter but the model assumes symmetry, the expression to fit to the experimental data can be constructed combining $c_s\,(1-2x)$ and $c_s\,(2x-1)$, where x is the fraction of cast thickness, and

$$c_s(r) = \frac{a}{1+br^3}, \quad \text{where} \quad a = \alpha m_l \ \text{ and } \ b = \frac{3m_l\rho}{c_0 k\mathrm{StLe}}. \tag{7.4}$$

https://doi.org/10.1017/S095679252000011X Published online by Cambridge University Press

We find that the values $a \approx 0.03$ and $b \approx 8$ give reasonable agreements between the experimental data and the asymptotic results as shown in Figure 7; no additional parameter fitting was employed. The noise in the data is inherent to the experimental measurements, and it is caused by the microstructure configurations. Still, we find a direct comparison better than artificially cleaning the data. Despite the noise in the measurements, we can still observe a certain trend in the concentration: increasing from the boundaries to the interior, and then a region of roughly constant concentration at the centre of the domain. This trend agrees with the behaviour predicted by (7.4), therefore our simple model helps us to better understand the underlying trend, even though the data are rather noisy.

8 Discussion

In this paper, we have considered the solidification problem of a binary alloy in a spherical domain. Since closed-form exact solutions cannot be found, we have performed an asymptotic expansion in large Lewis number limit and then in small Stefan number (which is valid for $\mathrm{Le}^{-\frac{2}{3}} \ll \mathrm{St}$). We also made the following assumptions: small diffusivity of impurities in the solid, segregation coefficient, initial concentration and initial temperature and large supercooling coefficient. We distinguished eight different layers over three time regimes. The dynamics of the early stage of the problem are similar to the problem for the pure material described in [30], as the supercooling effects are small. The impurities are rejected into the liquid phase and diffuse away over a very short length scale. For this geometry, we observed that the concentration at the interface does not remain constant but grows in time. It is this growth which leads to the second regime, around the critical time $t^* \approx \frac{\rho}{6k\mathrm{St}} + \frac{1}{6\kappa}$. In this regime, the concentration of impurities has become large enough to cause a significant change in the melting temperature, resulting in a change in the thermal problem and a deceleration of the moving boundary. At late times, the temperature of the whole system has reached the minimum temperature and thus the thermal problem remains in steady state, implying that the interfacial concentration stays constant. Then, we need to solve the one-phase Stefan problem for the diffusion of impurities in a shrinking core, in order to find the concentration in the liquid and the position of the interface, which has to be solved numerically. The asymptotic solutions show good agreement with the numerical simulations. We also compare the asymptotic solutions with experimental data provided by Elkem for silicon granules. By choosing a suitable parameter set, we find good agreement between the experiments and the asymptotic solution, therefore the results presented here can be used to better understand the water granulation casting process.

The analysis highlights the crucial role of constitutional supercooling in the behaviour of the system, even though its contribution was assumed to be small in the model. It is constitutional supercooling which triggers regime ii, and thus we observe a different behaviour to that described in previous works on the solidification of pure materials [30, 37, 39], or in [15], where supercooling was taken to be much smaller so that it fully decoupled from the thermal problem. Compared with the finite planar geometry studied in [4], we also observe a change of the order of the regimes, and hence the boundary layer structure. For the sphere, we first see the supercooling effects bring the temperature of the system down to the minimal temperature and slow the motion of the interface, and later the diffusion of impurities in the liquid region to the homogeneous steady state.

https://doi.org/10.1017/S095679252000011X Published online by Cambridge University Press

Even though the model is quite simple and the available experimental data are noisy, we have shown that the matched asymptotic solutions to the model are able to capture the underlying qualitative trend in the data. In terms of practical application, the model provides insight on the timescale required for solidification (in the model, this is the timescale until regime iii). The model also shows the effect of the impurities on the solidification process and, in particular, how these impurities are distributed along the particle radius. This distribution can be useful for further analysis on the properties of the solidified material, which may be linked to the microstructure of the solidified material, at least in an empirical manner. Our results can be used to determine how long the particles need to be cooled until they have solidified, as well as the influence of each parameter on the final solidification time and impurity distribution within the particle. In turn, this may enable our industrial partners to perform additional experiments using certain parameter groups as control parameters, in order to improve their approach to silicon manufacture through the water granulation process.

One could extend this work considering other aspects of the symmetric problem. A possible extension is to determine higher order asymptotic solutions, in order to increase the accuracy of our approximations; however, we suspect that this will require one to consider other layers and the problem complexity will increase, similarly to what was shown in other work [30, 37, 39]. Other extensions would be to consider a more general geometry and extend the analysis of McCue et al. [29] to binary alloys. One could perform a similar asymptotic analysis for other special geometries, such as a cylinder, which should be conceptually similar to the sphere. Finally, one might also consider a stability analysis for the spherical problem, or other three-dimensional geometries, akin to what we did for infinite and semi-infinite planar domain problems, in [3].

Conflict of Interest

None.

Acknowledgements

This publication is based on work supported by the EPSRC Centre For Doctoral Training in Industrially Focused Mathematical Modelling (EP/L015803/1) in collaboration with Elkem ASA. F. Brosa Planella is grateful to Elkem ASA for the financial support and the opportunity to work on site. We thank A. Autruffe, K. Hildal, S. D. Howison, B. Kroka, A. A. Lacey and A. Valderhaug for useful comments and discussions and A. A. Eftekhari for support with FVToolbox.

References

[1] Allen, D. N. D. G. & Severn, R. T. (1952) The application of relaxation methods to the solution of non-elliptic partial differential equations: II. The solidification of liquids. *Q. J. Mech. Appl. Math.* **5**(4), 447–454.

[2] Benham, G. P., Hildal, K., Please, C. P. & Van Gorder, R. A. (2016) Solidification of silicon in a one-dimensional slab and a two-dimensional wedge. *Int. J. Heat Mass Transfer* **98**, 530–540.

[3] Brosa Planella, F., Please, C. P. & Van Gorder, R. A. (2018) Instability in the self-similar motion of a planar solidification front. *IMA J. Appl. Math.* **83**(1), 106–130.

[4] Brosa Planella, F., Please, C. P. & Van Gorder, R. A. (2019) Extended Stefan problem for solidification of binary alloys in a finite planar domain. *SIAM J. Appl. Math.* **79**(3), 876–913.

[5] CHADAM, J., HOWISON, S. & ORTOLEVA, P. (1987) Existence and stability for spherical crystals growing in a supersaturated solution. *IMA J. Appl. Math.* **39**(1), 1–15.
[6] CHEN, S., MERRIMAN, B., OSHER, S. & SMEREKA, P. (1997) A simple level set method for solving Stefan problems. *J. Comput. Phys.* **135**(1), 8–29.
[7] CRANK, J. & GUPTA, R. S. (1975) Isotherm migration method in two dimensions. *Int. J. Heat Mass Transfer* **18**(9), 1101–1107.
[8] CROWLEY, A. B. (1978) Numerical solution of Stefan problems. *Int. J. Heat Mass Transfer* **21**(2), 215–219.
[9] DAVIS, G. B. AND HILL, J. M. (1982) A moving boundary problem for the sphere. *IMA J. Appl. Math.* **29**(1), 99–111.
[10] EFTEKHARI, A. A. & SCHÜLLER, K. (2018) FVTool: a finite volume toolbox for Matlab. https://github.com/simulkade/FVTool.
[11] ELLIOTT, C. M. & OCKENDON, J. R. (1982) *Weak and Variational Methods for Moving Boundary Problems*, Vol. 59, Pitman Publishing, Boston.
[12] FASANO, A., PRIMICERIO, M., HOWISON, S. D. & OCKENDON, J. R. (1989) On the singularities of one-dimensional stefan problems with supercooling. In: J. F. Rodrigues (editor) *Mathematical Models for Phase Change Problems*. International Series of Numerical Mathematics, Vol 88, Birkhäuser Basel, Springer, pp. 215–226.
[13] FASANO, A., PRIMICERIO, M., HOWISON, S. D. & OCKENDON, J. R. (1990) Some remarks on the regularization of supercooled one-phase Stefan problems in one dimension. *Q. Appl. Math.* **48**(1), 153–168.
[14] FASANO, A., PRIMICERIO, M. & LACEY, A. A. (1981) New results on some classical parabolic free-boundary problems. *Q. Appl. Math.* **38**(4), 439–460.
[15] FELTHAM, D. L. & GARSIDE, J. (2001) Analytical and numerical solutions describing the inward solidification of a binary melt. *Chem. Eng. Sci.* **56**(7), 2357–2370.
[16] GUPTA, S. C. (1990) Numerical and analytical solutions of one-dimensional freezing of dilute binary alloys with coupled heat and mass transfer. *Int. J. Heat Mass Transfer*, **33**(4), 593–602.
[17] HERRERO, M. A. & VELÁZQUEZ, J. J. L. (1996) Singularity formation in the one-dimensional supercooled Stefan problem. *Eur.J.Appl. Math.* **7**(2), 119–150.
[18] HILL, J. M. & KUCERA, A. (1983a) Freezing a saturated liquid inside a sphere. *Int. J. Heat Mass Transfer* **26**(11), 1631–1637.
[19] HILL, J. M. & KUCERA, A. (1983b) The time to complete reaction or solidification of a sphere. *Chem. Eng. Sci.* **38**(8), 1360–1362.
[20] HOWISON, S. (1988) Similarity solutions to the Stefan problem and the binary alloy problem. *IMA J. Appl. Math.* **40**(3), 147–161.
[21] JAAFAR, M. A., ROUSSE, D. R., GIBOUT, S. & BÉDÉCARRATS, J.-P. (2017) A review of dendritic growth during solidification: mathematical modeling and numerical simulations. *Renewable Sustainable Energy Rev.* **74**, 1064–1079.
[22] JIJI, L. M. & WEINBAUM, S. (1978) Perturbation solutions for melting or freezing in annular regions initially not at the fusion temperature. *Int. J. Heat Mass Transfer* **21**(5), 581–592.
[23] KING, J. R., RILEY, D. S. & WALLMAN, A. M. (1999) Two–dimensional solidification in a corner. *Proc. R. Soc. London A Math. Phys. Eng. Sci.* **455**(1989), 3449–3470.
[24] KUCERA, A. & HILL, J. M. (1986) On inward solidifying cylinders and spheres initially not at their fusion temperature. *Int. J. Non-linear Mech.* **21**(1), 73–82.
[25] LAMÉ, G. & CLAPEYRON, B. P. E. (1831) Mémoire sur la solidification par refroidissement d'un globe liquide. *Annales Chimie Physique* **47**, 250–256.
[26] LAZARIDIS, A. (1970) A numerical solution of the multidimensional solidification (or melting) problem. *Int. J. Heat Mass Transfer* **13**(9), 1459–1477.
[27] LIU, F. & MCELWAIN, D. L. S. (1997) A computationally efficient solution technique for moving-boundary problems in finite media. *IMA J. Appl. Math.* **59**(1), 71–84.
[28] MCCUE, S. W., KING, J. R. & RILEY, D. S. (2003) Extinction behaviour for two–dimensional inward-solidification problems. *Proc. R. Soc. London A Math. Phys. Eng. Sci.* **459**(2032), 977–999.

[29] McCue, S. W., King, J. R. & Riley, D. S. (2005) The extinction problem for three-dimensional inward solidification. *J. Eng. Math.* **52**(4), 389–409.
[30] McCue, S. W., Wu, B. & Hill, J. M. (2008) Classical two-phase Stefan problem for spheres. *Proc. R. Soc. London A Math. Phys. Eng. Sci.* **464**(2096), 2055–2076.
[31] Nelson, L., Brooks, P., Bonazza, R., Corradini, M., Hildal, K. & Bergstrom, T. (2005) Steam explosions of single drops of molten silicon-rich alloys. In: *Proceedings of the Ninth International Ferroalloys Congress (INFACON 9)*, pp. 338–351.
[32] Nygaard, L., Brekken, H., Lie, H., Magnussen, T. E. & Sveine, A. (1995) Water granulation of ferrosilicon and silicon metal. In: *INFACON 7, Trondheim, Norway*, pp. 665–671.
[33] Pedroso, R. I. & Domoto, G. A. (1973) Perturbation solutions for spherical solidification of saturated liquids. *J. Heat Transfer* **95**(1), 42–46.
[34] Riley, D. S., Smith, F. T. & Poots, G. (1974) The inward solidification of spheres and circular cylinders. *Int. J. Heat Mass Transfer* **17**(12), 1507–1516.
[35] Rubinstein, L. I. (1971) *The Stefan Problem*, Translations of Mathematical Monographs, Vol. 27, American Mathematical Society, Providence, Rhode Island.
[36] Selim, M. S. & Seagrave, R. C. (1973) Solution of moving-boundary transport problems in finite media by integral transforms. II. Problems with a cylindrical or spherical moving boundary. *Ind. Eng. Chem. Fundam.* **12**(1), 9–13.
[37] Soward, A. M. (1980) A unified approach to Stefan's problem for spheres and cylinders. *Proc. R. Soc. London A Math. Phys. Eng. Sci.* **373**(1752), 131–147.
[38] Stefan, J. (1890) Über die Theorie der Eisbildung. *Monatshefte für Mathematik* **1**(1), 1–6.
[39] Stewartson, K. & Waechter, R. T. (1976) On Stefan's problem for spheres. *Proc. R. Soc. London Ser. A Math. Phys. Sci.* **348**(1655), 415–426.
[40] Tao, L. C. (1967) Generalized numerical solutions of freezing a saturated liquid in cylinders and spheres. *AIChE J.* **13**(1), 165–169.
[41] Theillard, M., Gibou, F. & Pollock, T. (2015) A sharp computational method for the simulation of the solidification of binary alloys. *J. Sci. Comput.* **63**(2), 330–354.
[42] Van Dyke, M. (1975) *Perturbation Methods in Fluid Mechanics*, Parabolic Press, Stanford, California.
[43] Voller, V. & Cross, M. (1981) Accurate solutions of moving boundary problems using the enthalpy method. *Int. J. Heat Mass Transfer* **24**(3), 545–556.
[44] Wallman, A. M., King, J. R. & Riley, D. S. (1997) Asymptotic and numerical solutions for the two-dimensional solidification of a liquid half-space. *Proc. R. Soc. London A Math. Phys. Eng. Sci.* **453**(1962), 1397–1410.
[45] Wang, G.-X., Prasad, V. & Matthys, E. F. (1997) An interface-tracking numerical method for rapid planar solidification of binary alloys with application to microsegregation. *Mater. Sci. Eng. A*, **225**(1–2), 47–58.
[46] Wheeler, A. A., Boettinger, W. J. & McFadden, G. B. (1993a) Phase-field model of solute trapping during solidification. *Phys.Rev. E*, **47**(3), 1893.
[47] Wheeler, A. A., Murray, B. T. & Schaefer, R. J. (1993b) Computation of dendrites using a phase field model. *Phys. D Nonlinear Phenom.* **66**(1–2), 243–262.
[48] Yang, J., Zhao, C.-Y. & Hutchins, D. (2012) Modelling the effect of binary phase composition on inward solidification of a particle. *Int. J. Heat Mass Transfer* **55**(23), 6766–6774.

Appendix: Numerical scheme

In order to solve (2.2) numerically, we choose a fixed boundary scheme as it was done in [4] for the planar geometry. The key idea is the following: rescale solid and liquid regions so that they have fixed boundaries. We ensure that the algorithm conserves mass of impurities.

https://doi.org/10.1017/S095679252000011X Published online by Cambridge University Press

We introduce the variable $x = \frac{r-S(t)}{1-S(t)}$ for the solid phase and $y = \frac{r}{S(t)}$ for the liquid phase, which are both defined in the domain $[0, 1]$. In order to write the system in conservation form, we define the following quantities:

$$\begin{aligned} \phi_1(t,x) &= \left(x + \frac{S(t)}{1-S(t)}\right)^2 (1-S(t))^3 c_s(t,x), \qquad \phi_3(t,y) = S(t)^3 c_l(t,y), \\ \phi_2(t,x) &= \left(x + \frac{S(t)}{1-S(t)}\right)^2 (1-S(t))^3 T_s(t,x), \qquad \phi_4(t,y) = S(t)^3 T_l(t,y), \end{aligned} \tag{A1}$$

so that we can rewrite the system (2.2) in the following way. In the solid phase $x \in (0, 1)$, we have

$$\frac{\partial \phi_1}{\partial t} = \frac{\partial}{\partial x}\left(\left(\frac{S'(t)}{1-S(t)}(1-x) - \frac{2D\mathrm{Le}^{-1}}{\left(x + \frac{S(t)}{1-S(t)}\right)(1-S(t))^2}\right)\phi_1 + \frac{D\mathrm{Le}^{-1}}{(1-S(t))^2}\frac{\partial \phi_1}{\partial x}\right), \tag{A2a}$$

$$\frac{\partial \phi_2}{\partial t} = \frac{\partial}{\partial x}\left(\left(\frac{S'(t)}{1-S(t)}(1-x) - \frac{2\kappa}{\left(x + \frac{S(t)}{1-S(t)}\right)(1-S(t))^2}\right)\phi_2 + \frac{\kappa}{1-S(t)^2}\frac{\partial \phi_2}{\partial x}\right). \tag{A2b}$$

In the liquid phase $y \in (0, 1)$, we have

$$\frac{\partial \phi_3}{\partial t} + \frac{1}{y^2}\frac{\partial}{\partial y}\left[y^2\left(-\frac{S'(t)}{S(t)}y\phi_3 - \frac{1}{\mathrm{Le}S(t)^2}\frac{\partial \phi_3}{\partial y}\right)\right] = 0, \tag{A2c}$$

$$\frac{\partial \phi_4}{\partial t} + \frac{1}{y^2}\frac{\partial}{\partial y}\left[y^2\left(-\frac{S'(t)}{S(t)}y\phi_4 - \frac{1}{S(t)^2}\frac{\partial \phi_4}{\partial y}\right)\right] = 0. \tag{A2d}$$

At the interface, given by $x = 0$ and $y = 1$, we have

$$S(t)\phi_2 = (1-S(t))\phi_4, \quad S(t)\phi_1 = \alpha(1-S(t))\phi_3, \quad \phi_3 = -m_l\phi_4, \tag{A2e}$$

$$\frac{\rho}{\mathrm{St}}\frac{\mathrm{d}S}{\mathrm{d}t} = \frac{k}{(1-S(t))^2S(t)^2}\frac{\partial \phi_2}{\partial x} - \frac{2k}{(1-S(t))S(t)^3}\phi_2 - \frac{1}{S(t)^4}\frac{\partial \phi_4}{\partial y}, \tag{A2f}$$

$$\begin{aligned} &\left(-\frac{S'(t)}{(1-S(t))S(t)^2} + \frac{2D}{\mathrm{Le}(1-S(t))S(t)^3}\right)\phi_1 - \frac{D}{\mathrm{Le}(1-S(t))^2S(t)^2}\frac{\partial \phi_1}{\partial x} \\ &\quad = -\frac{S'(t)}{S(t)}\phi_3 - \frac{1}{\mathrm{Le}S(t)^2}\frac{\partial \phi_3}{\partial y}. \end{aligned} \tag{A2g}$$

The boundary conditions are

$$\frac{\partial \phi_3}{\partial y} = \frac{\partial \phi_4}{\partial y} = 0 \quad \text{at } y = 0, \tag{A2h}$$

$$\frac{\partial \phi_1}{\partial x} = 2(1-S(t))\phi_1 \quad \text{and} \quad \phi_2 = -(1-S(t)) \quad \text{at } x = 1, \tag{A2i}$$

and we prescribe the corresponding initial conditions for ϕ_1, ϕ_2, ϕ_3, ϕ_4 and S. Notice that if we start with a liquid phase only, this means $S \to 1$, so that $x \to \infty$. In order to avoid this singularity, we initialise the problem with a thin layer of solid near $S = 1$, and we use the early-time solutions calculated as the initial conditions.

https://doi.org/10.1017/S095679252000011X Published online by Cambridge University Press

To avoid numerical instabilities, we use a total variation diminishing discretisation for the advection term, and we implement the finite volume scheme in Matlab using FVToolbox [10]. Since α is very small, we take $\alpha = 0$, and therefore we neglect the impurities in the solid, considering only impurities in the liquid when performing our simulations. This reduces the condition (A2f) to a no-flux condition and removes equation (A2a) as well as the middle condition in (A2d) from the system. At each time step, we iterate using a relaxation scheme until convergence as described in [4].

https://doi.org/10.1017/S095679252000011X Published online by Cambridge University Press